Formation of kyanite-quartz veins of the Alpe Sponda, Central Alps, Switzerland

implications for Al transport during regional metamorphism

Originally published in:
Contributions to Mineralogy and Petrology 156(6), https://doi.org/10.1007/s00410-008-0310-4

Contrib Mineral Petrol (2008) 156:689–707
DOI 10.1007/s00410-008-0310-4

ORIGINAL PAPER

Formation of kyanite–quartz veins of the Alpe Sponda, Central Alps, Switzerland: implications for Al transport during regional metamorphism

Thorsten Beitter · Thomas Wagner · Gregor Markl

Received: 5 November 2007 / Accepted: 7 May 2008 / Published online: 27 May 2008

Abstract In this study, we have investigated the formation of quartz–kyanite veins of the Alpe Sponda, Central Alps, Switzerland. We have integrated field observations, fluid inclusion and stable isotope data and combined this with numerical geochemical modeling to constrain the chemical processes of aluminum transport and deposition. The estimated P–T conditions of the quartz–kyanite veins, based on conventional geothermometry (garnet–biotite, white mica solvus and quartz–kyanite oxygen isotope thermometry) and fluid inclusion data, are 550 ± 30°C at 5.0 ± 0.5 kbar. Geochemical modeling involved construction of aqueous species predominance diagrams, calculation of kyanite and quartz solubility, and reaction–path simulations. The results of the modeling demonstrate that (1) for the given chemical composition of the vein-forming fluids mixed Al–Si aqueous species are dominant in transporting Al, and that (2) fluid cooling along a small temperature gradient coupled with a pH decrease is able to explain the precipitation of the quartz–kyanite assemblages in the proportions that are observed in the Alpe Sponda veins. We conclude that sufficient amounts of Al can be transported in typical medium- to high-grade regional metamorphic fluids and that immobile behavior of Al is not very likely in advection–dominanted fluid–rock systems in the upper and middle crust.

Keywords Kyanite · Aluminum solubility · Aluminum mobility · Alpe Sponda · Metamorphism

Communicated by J. Hoefs.

T. Beitter · G. Markl
Institut für Geowissenschaften,
Arbeitsbereich Mineralogie und Geodynamik,
Wilhelmstr. 56, 72074 Tubingen, Germany

T. Wagner (✉)
Institute of Isotope Geochemistry and Mineral Resources,
ETH Zürich, NW F 82.4, Clausiusstrasse 25,
8092 Zurich, Switzerland
e-mail: thomas.wagner@erdw.ethz.ch;
th.wagner@uni-tuebingen.de

Introduction

The extent of aluminum mobility during regional metamorphism and fluid–rock interaction has been the subject of ongoing discussions in the petrological literature. Earlier studies, amongst them the important work of Carmichael (1969), have concluded that aluminum is generally relatively immobile compared to other elements (such as the alkalies, Ca, Mg and Fe) during fluid–rock interaction (Ragnarsdottir and Walther 1985; Verdes et al. 1992). Therefore, it has been extensively used as a constant reference frame for mass balance calculations in studies of mass transfer during regional metamorphism (Thompson 1975; Ferry 1987, 1988; Grant 1986) and hydrothermal alteration (Lentz and Gregoire 1995). Based on field observations such as the widespread occurrence of alumosilicate-rich veins and segregations in regionally metamorphosed pelites (Widmer and Thompson 2001; Putlitz et al. 2002), acid hydrothermal alteration styles (Kelepertsis and Esson 1987; Rubin et al. 1993), as well as eclogites and other high-pressure metamorphic rocks (Franz et al. 2001; Masters and Ague 2005), this assumption has been repeatedly challenged. It was proposed that aluminum must have a higher solubility at elevated temperatures and pressures and can be transported in significant amounts in aqueous crustal fluids (Yardley 1977; Kerrick 1988).

Subsequent experimental and numerical studies of the behavior of aluminum in fluid–rock systems have generally substantiated the concept of enhanced Al solubility at elevated P–T conditions (Manning 1998, 2006, 2007; Pokrovski et al. 1998; Zaraisky and Soboleva 1997; Newton and Manning 2007, 2008). These studies have demonstrated that (1) the solubility of aluminum in aqueous fluids under upper- to mid-crustal conditions is significantly higher than previously assumed due to the formation of stable Al complexes with a number of inorganic ligands (Salvi et al. 1998; Tagirov and Schott 2001; Tagirov et al. 2002, 2004; Manning 2006, 2007), and (2) that aluminum diffusion along a strong chemical potential gradient can be also important for Al transport on a local scale (Widmer and Thompson 2001). Despite this considerable progress in the understanding of Al transport and mobility in crustal fluids, the currently available data and models are not yet able to fully explain the formation of alumosilicate veins and segregations.

One important question that needs to be resolved is the relative enrichment in alumosilicate minerals observed in such veins, compared to the abundance of quartz and other silicate and oxide phases. The high solubility of Al required for precipitating sufficiently large amounts of alumosilicate minerals from aqueous metamorphic fluids as a response to changes in temperature, pressure or chemical potential cannot be achieved through a speciation model that includes only Al hydroxide and alkali aluminate complexes (Pokrovskii and Helgeson 1995, 1997; Diakonov et al. 1996; Tagirov and Schott 2001; Verlaguet et al. 2006; Tropper and Manning 2007). Such high solubilities require the involvement of additional factors such as (1) elevated concentrations of unusual ligands, e.g. fluorine or boron, that would result in the formation of large amounts of Al fluoride and borate complexes which are very stable at elevated temperatures (Tagirov and Schott 2001; Tagirov et al. 2004), or (2) a substantial extent of Al–Si complexing in metamorphic fluids, which appears quite plausible based on the limited experimental data that are available (Pokrovski et al. 1996, 1998; Salvi et al. 1998; Manning 2007; Newton and Manning 2007). A considerable amount of experimental work on Al–Si complex stability has been performed at temperatures below 300°C and relatively low pressures (Pokrovski et al. 1996, 1998; Salvi et al. 1998), whereas only a single experimental study has directly addressed the solubility of quartz–alumosilicate assemblages at metamorphic P–T conditions (Manning 2007).

Encouraged by the increasing availability of experimental Al solubility and complex stability data, we have developed a comprehensive speciation model for Al transport in aqueous metamorphic fluids up to temperatures and pressures of 600°C and 5 kbar. We have applied this model to derive the conditions and processes that were important for the formation of quartz–kyanite veins exposed in amphibolite–grade gneisses of the Alpe Sponda, Central Alps (Switzerland), one of the classic localities where such veins have been described (Klein 1976; Irouschek 1983; Kerrick 1988; Todd and Engi 1997). We first determine the metamorphic pressure–temperature conditions prevalent during formation of the quartz–kyanite veins through combination of conventional geothermobarometry, oxygen isotope and fluid inclusion studies. These data are then used to model solubility, transport and precipitation of aluminum and silica in aqueous fluids, using various speciation and reaction–path calculations. Based on the results of these simulations, we suggest simple (isobaric) cooling along a small temperature gradient coupled with a pH decrease as the most likely vein-forming mechanism. Our model is able to quantitatively explain both the mineral assemblage and the relative mineral proportions in the quartz–kyanite veins, whereas formation of kyanite–mica lenses requires additional factors such as enhanced fluid–rock interaction resulting in dissolution of quartz and ferromagnesian minerals.

Geological setting

The kyanite occurrences of the Alpe Sponda are located in the north-western part of the Simano Nappe, Central Alps, Switzerland (Fig. 1). The Simano Nappe is one of the

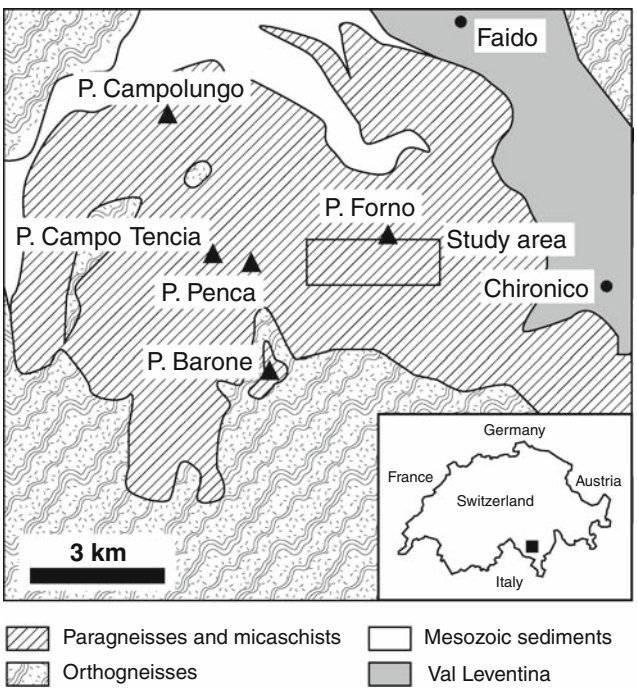

Fig. 1 Geological sketch map of the Simano nappe complex, Central Alps, showing the location of the studied quartz–kyanite veins and kyanite–mica lenses

tectonically lower Alpine Nappes and belongs to the lower Penninic units (Rütti 2003). This nappe complex belonged, like the adjacent Leventina, Maggia, Adula, and Cima Lunga units, to the Penninc Ocean prior to its subduction. This ocean, separating the European and African continental margin, was subdivided into two main units, which are (1) the South Penninic Ocean and Middle Penninic continental shelf, together also referred to as upper Penninic units, and (2) the North Penninic Ocean, the lower Penninc units (Milnes 1974; Frisch 1979; Frisch and Meschede 2005; Maxelon and Mancktelow 2005). Southward-directed subduction commenced in the Cretaceous and culminated in continental collision approximately 35 million years (Ma) ago (Frisch 1979; Frisch and Meschede 2005). Today the nappe complex that was formed through this collision process can be found between the Gotthard Massif in the north and the Insubric Line near Bellinzona in the south. The Simano nappe, in which the Alpe Sponda is situated, is part of this nappe complex.

The metamorphic conditions in this region have mainly attained amphibolite–facies conditions (Frey and Mählmann 1999). In contrast to the Cima Lunga unit, no evidence for an Eoalpine high-P or ultrahigh-P metamorphism has yet been found in the Simano nappe (Rütti et al. 2005). Peak temperatures increase southward from approximately 500–700°C at the Insubric Line, whereas maximum pressures of approximately 7 kbar were attained along an elongate zone between the Gotthard Massif and the Insubric Line, decreasing systematically towards the north and south (Todd and Engi 1997). In major parts of this region staurolite and kyanite assemblages are stable, whereas sillimanite occurs only in a narrow zone close to the Insubric line (Niggli 1970; Todd and Engi 1997). The Simano Nappe consists mainly of various types of ortho- and paragneisses (Maxelon and Mancktelow 2005). The north-west is dominated by pre-mesozoic staurolite-bearing paragneisses (Keller 1968). Peak metamorphic conditions in this area are estimated at 600–650°C and 6–6.5 kbar (Rütti et al. 2005; Todd and Engi 1997).

Samples and methods

A suite of representative samples of different quartz–kyanite veins, kyanite–mica lenses and host–rock gneisses were collected in the field. A subset of this sample material was selected for petrographic, electron-microprobe, fluid inclusion and stable isotope studies. Wavelength-dispersive electron-microprobe analysis was performed with a Jeol JXA 8900 RL instrument. The acceleration voltage was 15 kV and the beam current 20 nA. Both natural and synthetic standards were used for calibration. Peak counting times were 16 s for major and 30 s for minor elements. Fluorine was measured for 60 s, and a peak overlap correction was applied to account for the interference of the F–$K\alpha$ and Fe–$L\beta$ peaks. Background counting times were always half of the peak counting times. A ZAF matrix correction (Armstrong 1991) was applied to the raw data.

Fluid inclusions were studied in doubly polished sections and large single crystals of kyanite. Microthermometric measurements were carried out with a Linkham THMS-600 heating–cooling stage mounted on a Leica DMLP microscope. The system was calibrated using the triple point of pure CO_2 (−56.6°C) and melting and critical homogenization temperatures of pure H_2O (0°C and 374.1°C) of synthetic fluid inclusions. Heating rates were 0.1°C/min approaching phase transitions. Errors are assumed to be ± 0.2°C and ± 5°C for final ice melting and homogenization temperatures, respectively. The calculation of fluid inclusion properties was performed with the computer package FLUIDS (Bakker 2003), using appropriate equations of state for the H_2O–NaCl system to obtain bulk fluid densities (Zhang and Frantz 1987) and isochores (Bodnar and Vityk 1994; Knight and Bodnar 1989).

Fifteen samples of quartz, kyanite and rutile were analyzed for their oxygen isotope composition. Mineral separates were prepared by careful hand-picking under a binocular microscope, followed by cleaning in deionized water. Oxygen isotope analysis was performed using a laser extraction procedure that follows the techniques of Sharp (1992). The samples were heated with a CO_2 laser at a F_2 pressure of 50 mbar. The extracted O_2 was collected on a molecular sieve, subsequently expanded and $^{18}O/^{16}O$ was measured on a Finnigan MAT-252 gas source mass spectrometer. Reproducibility of the analytical results was monitored through replicate measurements of the international standard NBS-28 ($\delta^{18}O_{V\text{-}SMOW}$: +9.6‰). The analytical precision (1σ) was around ±0.3‰. All oxygen isotopic data are reported in standard delta notation, relative to V-SMOW.

Petrography

We have identified four distinct lithological units that are of importance for this study (Fig. 2). These are: (1) the host–rock paragneisses, (2) a narrow garnet-rich transition zone between host rocks and quartz–kyanite veins, (3) the quartz–kyanite veins (Fig. 3), and (4) the kyanite–mica lenses. Additional lithological units in the study area are recognized (lenses of orthogneisses, meta-gabbros, and amphibolites), but are not relevant to understanding the formation of the quartz–kyanite veins.

All quartz–kyanite veins and kyanite-mica lenses at the Alpe Sponda are located within paragneisses, which are

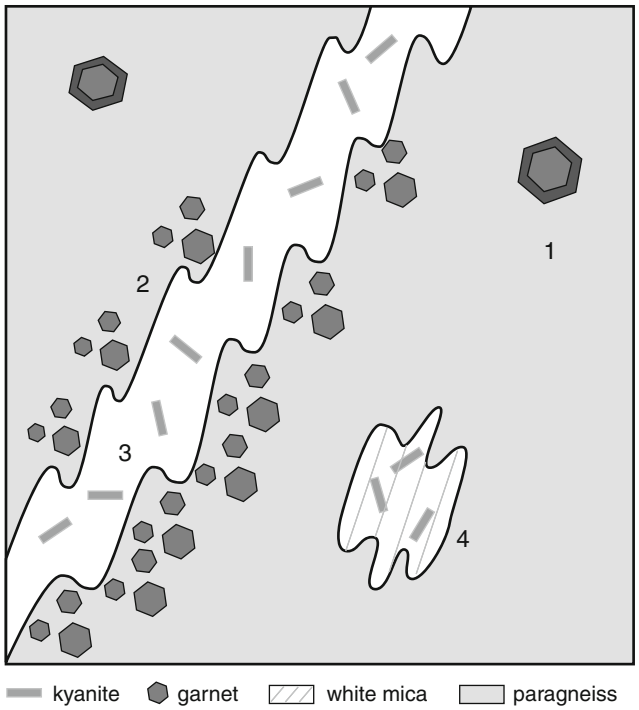

Fig. 2 Schematic sketch (not to scale) of the lithologies at the Alpe Sponda that are important for this study, which are (*1*) host–rock paragneisses with large, zoned garnet, (*2*) narrow transition zone rocks with small unzoned garnets, (*3*) quartz–kyanite veins, and (*4*) kyanite–mica lenses

particularly rich in staurolite, mica (biotite and muscovite-rich white mica), and plagioclase. Large, zoned garnets are frequently present (Fig. 4a) in the host rock gneisses distal to the veins and lenses. Accessory minerals in the gneisses are rutile, ilmenite, kyanite, and tourmaline. The narrow (1–2 cm in thickness) transition zone between the quartz–kyanite veins and the host rocks is commonly enriched in mica. In addition, small, unzoned garnets are, in places, quite abundant (Fig. 4b). Other minerals present are staurolite and kyanite. The modal composition of the host rock and the transition zone varies considerably, especially the modal contents of garnet and staurolite shows substantial variation. Therefore, it was not possible to establish reliable average modal compositions of the different rock types studied.

Field evidence demonstrates that the rock units of the Alpe Sponda area have experienced enhanced fluid flow and veining. Quartz veins that are mostly kyanite-bearing are very abundant (Fig. 3a, b). The average vein density that was observed is approximately 1–2 veins per five cubic meters of host rock, with significantly more veins occurring in places. The veins have lengths of 1–10 m and thicknesses of about 0.2–0.8 m. There are two distinct types of kyanite-bearing assemblages present at the Alpe Sponda, which are (1) quartz–kyanite veins and (2) kyanite–mica lenses. From the field relationships, it cannot be established that kyanite-bearing veins and the kyanite–mica lenses are related through the same fluid-assisted process. Rather, it appears that they constitute distinct assemblages that were formed via different mechanisms. Most likely the veins were formed through advective transport and deposition of solute material, whereas the lenses might be related to selective leaching of a suite of more soluble elements from the gneisses during fluid–rock interaction.

The veins generally consist only of quartz and kyanite (Fig. 4c), with the kyanite crystals making up about 4–5 vol.% of the veins. Rarely, the veins also contain large, cm-sized rutile crystals that appear to be not coeval with the kyanite. We have not observed any distinct selvages or pronounced zones of mineralogical and/or compositional changes adjacent to the veins that would correspond to alteration envelopes formed through extensive fluid–rock interaction in the wall rocks to the veins, although we note some enrichment in mica and garnet in the transition zone between host rocks and the veins. The quartz–kyanite veins are far more abundant than the kyanite-bearing lenses, which contain two texturally and chemically different types of white mica and less abundantly also the minerals biotite, plagioclase, and staurolite (Fig. 4d). Kyanite makes up to 8 vol.% of the lenses and the remaining fraction is composed of approximately equal amounts of muscovite and paragonite. Their dimensions do generally not exceed 0.5 m. Both types of kyanite assemblages have clearly

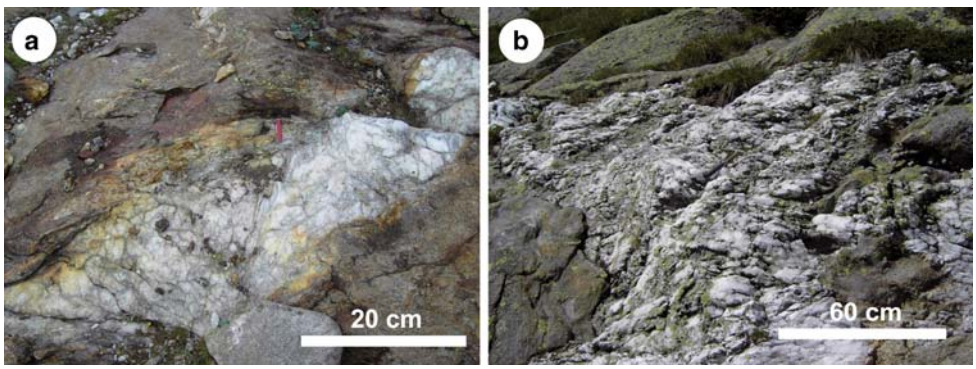

Fig. 3 Field relationships of kyanite bearing quartz veins. **a** Small deformed vein that is very rich in kyanite. **b** Larger, less deformed vein with only little kyanite visible

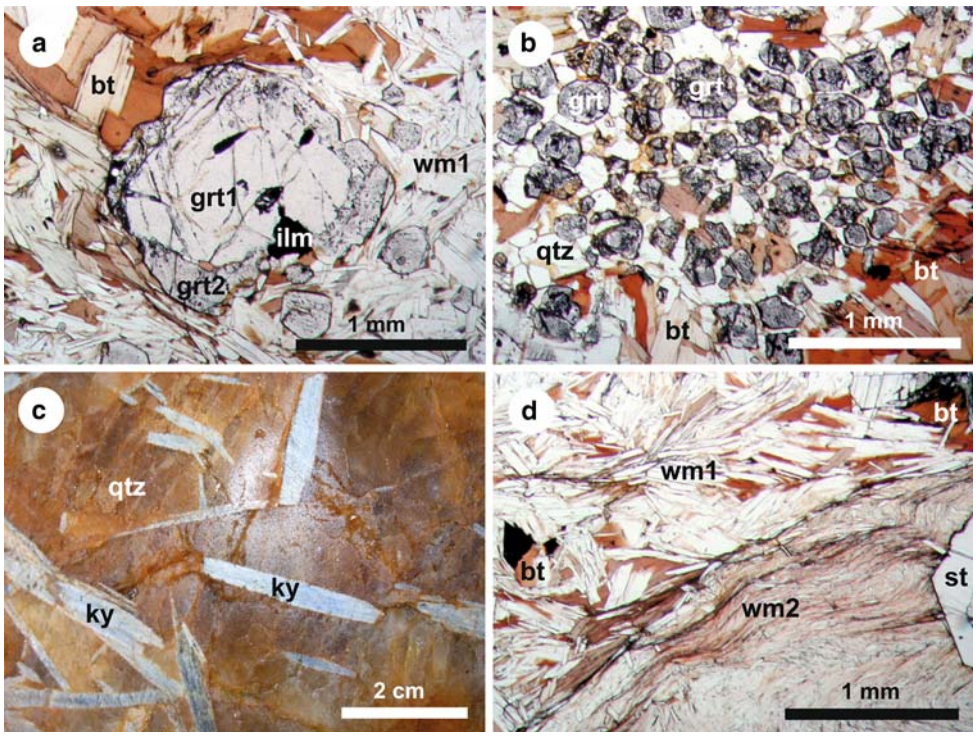

Fig. 4 Representative microphotographs of the typical kyanite-bearing assemblages and their host rocks, plane-polarized light. **a** Large, zoned host–rock garnet (*grt1* garnet core; *grt2* late garnet rim) with biotite (*bt*), white mica (*wm*), and inclusions of ilmenite (*ilm*). Sample: TU 19. **b** Typical small transition zone garnets with quartz (*qtz*). Sample: TB 34. **c** Quartz–kyanite vein. Sample: TB 37. **d** Kyanite–mica lens with coarse paragonite (*wm1*), fine-grained muscovite (*wm2*), and biotite (*bt*). Sample: TB 69

undergone tectonic deformation after their formation during the exhumation of the Simano Nappe, as shown by the microtextures.

Analytical results

Electron-microprobe analysis of large, zoned garnets in the host–rock gneisses show an increase in almandine and a decrease in grossular in the outermost rim (Fig. 5). The composition of the rims of the host–rock garnet is the same as the composition of the small garnet crystals that are present within the transition zone between the gneisses and the quartz–kyanite veins. White mica of the host–rock gneisses and the transition zone is texturally very similar and is muscovite that contains no more than 40 mol.% paragonite (Table 1). In contrast, white mica of the kyanite–mica lenses occurs as two different textural types, one being very fine-grained and the second one more coarse-grained. The coarse-grained white micas are muscovite similar to those of the host–rock gneisses and the transition zone, whereas the fine-grained mica is paragonite, with X_{Na} in the range 0.88–0.94 (Fig. 6). Biotite is mainly present within the host–rock gneisses and the transition zone, whereas it occurs only very rarely in the kyanite–mica lenses. All biotite shows texturally and chemically very little variation. The X_{Si} varies between 0.9 and 0.93 and X_{Mg} between 0.48 and 0.58. Biotite contains up to 0.15 atoms per formula unit (apfu) fluorine (based on 11 anhydrous oxygen atoms). The composition of all other analyzed minerals (staurolite, feldspar, chlorite) shows only very little variability.

The oxygen isotope composition of both quartz and kyanite from quartz–kyanite veins is rather homogeneous, with $\delta^{18}O$ values being in the range of 9.6–10.8‰ (average: 10.2 ± 0.5 ‰) and 6.9–7.9‰ (7.4 ± 0.4‰), respectively (Table 2). The $\delta^{18}O$ values of quartz and kyanite from kyanite–mica lenses are very similar to those from the veins. Rutile, which was analyzed from three quartz veins, has $\delta^{18}O$ values in the range of 1.8–2.2‰.

A summary of the fluid inclusion types observed and the corresponding microthermometric data is given in Table 3. Fluid inclusions in vein-hosted kyanite are dominated by two types, which are (1) pseudo-secondary two-phase aqueous (H_2O–NaCl) fluid inclusions oriented along healed microfractures that do not crosscut grain boundaries (Fig. 7), and (2) secondary three-phase aqueous-carbonic inclusions (H_2O–CO_2–NaCl). The pseudo-secondary inclusions in kyanite are elongate and have degrees of fill of approximately 80 vol.%. The final ice melting and total homogenization temperatures of 34 inclusions of this type could be determined. Final ice melting temperatures are in the range of −3.1 to −1.1°C (average: −1.9 ± 0.4°C), corresponding to salinities of 1.9–5.1 wt.% eqv. NaCl (Fig. 8). The homogenization temperatures are in the range of 220–306°C (average: 250 ± 28°C). Secondary aqueous two-phase inclusions that show compositional characteristics similar to the

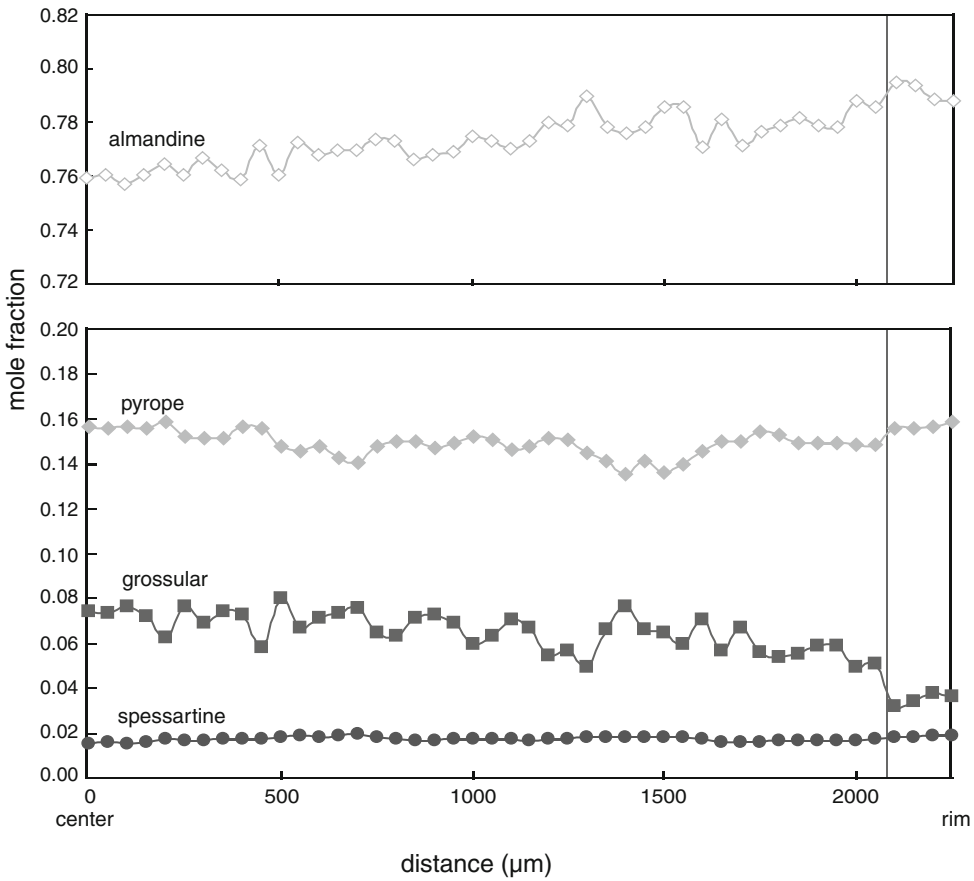

Fig. 5 Variation of end-member mole fraction of a single, zoned host–rock garnet along a line from centre to rim as analyzed with the microprobe. Distances between individual measurements were 50 μm. The transition from the core to the rim is indicated by a *vertical line*

pseudo-secondary inclusions in kyanite were found in the vein-hosted quartz as well. All calculations of P–T conditions and Al transport were based on the data of the kyanite hosted pseudo-secondary fluid inclusions, because they correspond most closely to the fluid that was responsible for the formation of the veins.

P–T-conditions of vein formation

We have utilized different geothermobarometric information (conventional cation exchange thermometry, stable isotope thermometry, fluid inclusion data) to estimate the P–T conditions of vein formation. These P–T estimates are then placed into the framework of available data on metamorphic peak conditions in the Simano nappe.

Garnet–biotite cation exchange (Mg–Fe) thermometry (Holdaway 2000) yields two different temperature ranges for the host–rock gneisses (Fig. 9). The garnet cores give 620 ± 30°C (1σ, based on a representative number of temperature calculations), if combined with the lowest Fe/Mg that was measured in the texturally coexisting biotite. The compositionally distinct rims of the host–rock garnets give 510 ± 25°C, combined with the average composition of the coexisting biotite. The approach we chose to calculate garnet–biotite temperatures was based on the assumption that, due to the high diffusivity of Fe and Mg, most of the biotite is in equilibrium with the latest formed garnet rims. Biotite domains that have the lowest Mg/Fe ratio have partly retained their original composition (in equilibrium with the garnet cores) that was established during peak metamorphism. The resulting temperatures represent, therefore, minimum values. Remarkably, we found that the smaller garnets in the transition zone to the quartz–kyanite veins, that were likely formed during the vein-forming event, give temperatures consistent with the rims of the larger host–rock garnets.

We interpret the two garnet–biotite temperatures as being related to two distinct events. The higher temperature reflects conditions close to peak metamorphism, because it corresponds well with available P–T estimates of the Simano Nappe and surrounding areas (Todd and Engi 1997; Rütti et al. 2005). The second, lower temperature is interpreted as being caused by a later, likely fluid-assisted event, that resulted in the growth of small garnets in the transition zone and diffusional re-equilibration of the biotite. Detailed geochronological studies in the nearby Lepontine area demonstrate that a post-peak thermal event has partially reset the geochronological systems. This thermal event, that occurred at around 29–25 Ma, has been interpreted as being

Table 1 Average electron-microprobe data of important minerals present in quartz–kyanite veins, kyanite–mica lenses and respective wallrocks, Alpe Sponda, Switzerland

Wt.%	Garnet	Staurolite	Biotite	White mica	Feldspar	Chlorite
SiO_2	37.6–39.0	27.6–28.7	36.0–38.7	45.8–48.6	61.4–65.1	24.7–26.2
Al_2O_3	21.0–22.0	52.8–55.1	18.2–20.1	34.5–40.4	21.6–25.0	21.9–24.1
MgO	2.75–4.39	1.36–2.43	10.2–12.4	0.07–1.03	b.d.	15.3–18.4
FeO	31.6–37.3	12.1–14.7	15.9–19.4	0.15–1.06	0–0.20	21.3–24.8
CaO	0.82–4.93	0–0.02	0–0.09	0–0.43	2.17–4.98	b.d.
MnO	0.57–5.07	0.06–0.35	0–0.17	b.d.	–	0.06–0.24
K_2O	–	–	7.55–9.32	0.93–1.69[a] 6.68–8.98[b]	0.07–0.29	b.d.
Na_2O	b.d.	b.d.	0.21–0.51	6.43–7.07[a] 1.53–3.04[b]	8.99–10.9	b.d.
TiO_2	0–1.29	0.25–0.83	1.29–1.91	0.03–0.56	–	0.04–0.16
F	–	–	0.14–0.59	0–0.03	–	b.d.
H_2O[c]	0	1.06–1.08	3.63–3.96	4.45–4.75	0	11.4–12.0
Apfu						
Si	2.97–3.03	7.80–8.02	2.69–2.79	2.98–3.17	2.70–2.87	2.57–2.70
Al	1.95–2.02	17.75–18.27	1.60–1.73	2.65–3.01	1.12–1.29	2.66–2.89
Mg	0.32–0.51	0.57–1.01	1.14–1.35	0.01–0.10	b.d.	2.38–2.75
Fe	2.06–2.44	2.82–3.52	0.97–1.22	0.01–0.06	0–0.01	1.80–2.14
Ca	0.07–0.41	0–0.01	0–0.01	0–0.03	0.10–0.23	b.d.
Mn	0.04–0.34	0.02–0.08	0–0.01	b.d.	b.d.	0–0.02
K	–	–	0.70–0.89	0.08–0.14[d] 0.55–0.76[e]	0–0.02	b.d.
Na	b.d.	b.d.	0.03–0.07	0.79–0.87[d] 0.19–0.38[e]	0.77–0.93	b.d
Ti	0–0.08	0.05–0.18	0.09–0.14	0–0.03	–	0–0.02
F	–	–	0.03–0.14	0–0.01	–	0–0.01
O[d]	12	23	11	11	8	14
H[e]	0	2	1.86–1.97	1.99–2.0	0	8

[a] Compositional range for paragonite solid-solutions

[b] Compositional range for muscovite solid-solutions

[c] Calculated

[d] Number of anhydrous oxygen atoms per formula unit used for the calculations

[e] H_2O Content was calculated from stoichiometry; the calculated H_2O content in biotite, chlorite and white mica was corrected for the analyzed F concentration

– Element was not analyzed

b.d.: Element concentration is below the detection limit

Standards and radiations used: Garnet and staurolite: pyrope (Si–$K\alpha$, Mg–$K\alpha$), SrTiO3 (Ti–$K\alpha$), plagioclase (Al–$K\alpha$), chromium metal (Cr–$K\alpha$), hematite (Fe–$K\alpha$), bustamite (Ca–$K\alpha$), rhodonite (Mn–$K\alpha$), and albite (Na–$K\alpha$). Biotite, white mica, and chlorite: diopside (Si–$K\alpha$, Mg–$K\alpha$), $SrTiO_3$ (Ti–$K\alpha$), plagioclase (Al–$K\alpha$), hematite (Fe–$K\alpha$), bustamite (Ca–$K\alpha$, Mn–$K\alpha$), albite (Na–$K\alpha$), zircon (Zr–$L\alpha$), sanidine (K–$K\alpha$), topaz (F–$K\alpha$), and tugtupite (Cl–$K\alpha$). Feldspar: albite (Si–$K\alpha$, Al–$K\alpha$, Na–$K\alpha$), hematite (Fe–$K\alpha$), bustamite (Ca–$K\alpha$), barite (Ba–$L\alpha$), celestite (Sr–$L\alpha$), and sanidine (K–$K\alpha$). Cr (for garnet and staurolite), Cl (biotite, white mica, chlorite), Sr and Ba (feldspar) were below the detection limit

related to extensive fluid circulation in the area (Gebauer 1999). It appears quite possible that this event correlates with the formation of the quartz–kyanite veins and the observed growth of both the small garnets in the transition zone and the garnet rims in the host–rock gneisses.

Comprehensive information on the temperatures during formation of the quartz–kyanite veins and the kyanite–mica lenses can be derived from the composition of coexisting muscovite and paragonite and from kyanite–quartz oxygen isotope thermometry. Applying solvus thermometry (Chatterjee and Flux 1986) for assumed pressures of 5–6 kbar, we have estimated equilibrium temperatures of 510 ± 80°C and 510 ± 50°C for paragonite and muscovite, respectively (Fig. 6). The different errors in

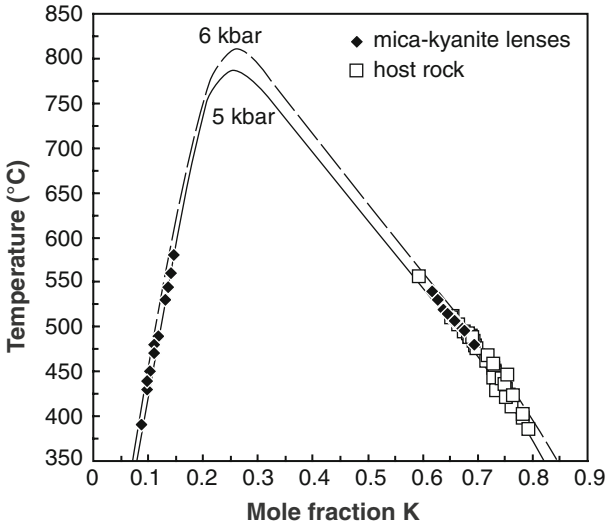

Fig. 6 Experimentally determined (Chatterjee and Flux 1986) muscovite–paragonite solvus in X_K–T space at 5 and 6 kbar with superimposed compositional data for white mica from kyanite–mica lenses and host rocks

Table 2 Oxygen isotope data for the analyzed quartz–kyanite veins, Alpe Sponda, Central Alps

Sample	Assemblage	Mineral	$\delta^{18}O_{V\text{-}SMOW}$
Rutile-bearing quartz veins			
TB 01	Qtz–rt	Qtz	10.4
TB 01	Qtz–rt	Rt	2.0
TB 65	Qtz–rt	Qtz	10.2
TB 65	Qtz–rt	Rt	2.2
TB 71	Qtz–rt	Qtz	9.6
TB 71	Qtz–rt	Rt	1.8
Quartz-kyanite veins			
TB 26	Qtz–ky	Qtz	10.5
TB 26	Qtz–ky	Ky	7.7
TB 37	Qtz–ky	Qtz	10.8
TB 37	Qtz–ky	Ky	7.9
TB 40	Qtz–ky–bt	Qtz	10.3
TB 46	Qtz–ky–st–bt	Qtz	10.2
TB 46	Qtz–ky–st–bt	Ky	7.1
TB 47	Qtz	Qtz	10.3
TB 66	Qtz–ky	Qtz	9.6
TB 66	Qtz–ky	Ky	6.9

Mineral abbreviations: *qtz* quartz, *ky* kyanite, *rt* rutile

temperature for the two white micas mainly results from the asymmetry of the solvus. The comparatively large range in X_{Na} (and the calculated solvus temperatures) of muscovite and paragonite could partly also result from progressive exsolution during retrograde cooling. If an empirical geothermometer for the muscovite–paragonite system (Blencoe et al. 1994) is applied, it yields different temperature estimates in the range of 620–690°C. These temperatures would conform to conditions of peak metamorphism that are well established for the Alpe Sponda. These considerably higher temperature estimates for kyanite–mica lenses are inconsistent with both the field relationships (that suggest formation of the lenses after peak metamorphism) and all other independent geothermometric information (garnet–biotite temperatures, stable isotope thermometry discussed below).

We calculated oxygen isotope equilibrium temperatures between quartz and kyanite, applying a number of different calibrations that are available in the literature (Richter and Hoernes 1988; Zheng 1993; Hoffbauer et al. 1994; Sharp 1995; Tennie et al. 1998). Three calibrations yield rather consistent isotope temperatures of 490 ± 30°C (Zheng 1993), 550 ± 30°C (Richter and Hoernes 1988), and 620 ± 30°C (Sharp 1995), which are well within the errors of the experimental and theoretical methods that were used to establish the respective fractionation factors. The remaining two calibrations (Hoffbauer et al. 1994; Tennie et al. 1998) gave equilibrium temperatures that are more than 100°C above the peak metamorphic conditions that were established for the Simano Nappe (Todd and Engi 1997; Rütti 2003). We have based our estimates of the P–T conditions of vein formation on the equilibrium temperatures that were obtained from the calibration of Richter and Hoernes (1988), because they represent the average of all three calibrations that gave consistent results (Fig. 9a). This selection is supported by oxygen isotope temperatures that were obtained from quartz–rutile pairs. Applying three different calibrations (Addy and Garlick 1974; Matthews 1994; Chacko et al. 1996), we have calculated a consistent temperature of 510 ± 20°C, which is identical within error with the average quartz–kyanite temperature.

Combining the different temperature estimates (garnet–biotite temperatures, white mica solvus temperatures, oxygen isotope exchange temperature) with isochores calculated for representative fluid inclusions hosted in kyanite, the P–T conditions during vein formation can be established. The pseudo-secondary fluid inclusions in kyanite show a systematic variation in homogenization temperatures (and also in the calculated density) at relatively constant salinity. This trend is interpreted to reflect a continuous density re-equilibration during exhumation of the veins (Sterner and Bodnar 1989). Therefore, the fluid inclusions with the highest densities (the lowest homogenization temperatures) reflect most closely the composition and density of the vein-forming fluid during trapping. The intercept of the isochores of these fluid inclusions with the oxygen isotope temperatures yields P–T conditions of 550 ± 30°C at 5.0 ± 0.4 kbar (Fig. 9).

Table 3 Summary of microthermometric data of fluid inclusions from quartz–kyanite veins and quartz–kyanite–mica lenses, Alpe Sonda, Central Alps

Samp.	Assemblage	Mineral	Type	*N*	T_m CO_2 (°C)	T_h CO_2 (°C)	$T_{m\ ice}$ (°C)	T_h (°C)
TB 37	Qtz–ky	Qtz	n.d.	22			−3.3 to −0.1	188–303
TB 40	Qtz–ky–bt	Qtz	n.d.	17			−3.7 to −0.1	150–330
TB 65	Qtz–rt	Qtz	n.d.	12			−4.0 to −0.1	151–287
TB 66	Qtz–ky	Qtz	n.d.	12			−3.5 to −0.7	190–284
TB 66	Qtz–ky	Ky	s.	3		29.8		257–288
Ky 1	Qtz–ky	Ky	ps.	8			−2.3 to −1.1	224–235
Ky 2	Qtz–ky	Ky	s.	3	−55.5 to −55.4	30.0 to 31.3		280–283
Ky 2	Qtz–ky	Ky	ps.	6			−1.9 to −1.2	220–236
Ky 3	Qtz–ky	Ky	n.d.	10			−3.3 to −0.1	281–333
Ky 4	Qtz–ky	Ky	ps.	12			−3.1 to −1.7	251–306

Qtz quartz, *ky* kyanite, *bt* biotite; *s* secondary, *ps* pseudosecondary, *n.d.* not determined. All samples were taken from quartz–kyanite veins, with the exception of Ky 2 and TB 65, that were taken from a kyanite–mica lens and a rutile-bearing quartz vein, respectively

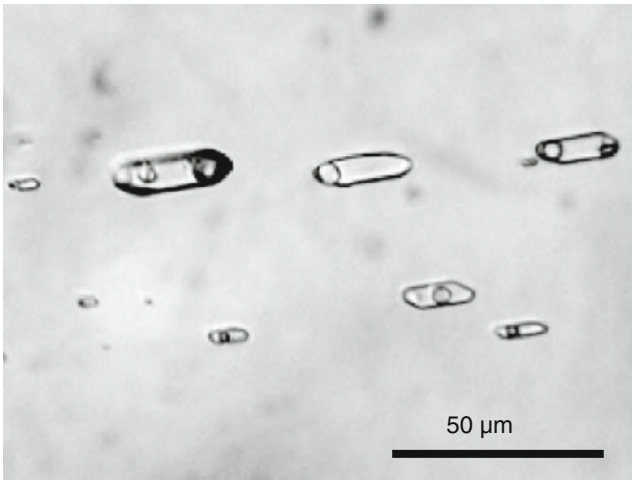

Fig. 7 Photomicrograph showing a typical trail of pseudo-secondary two-phase aqueous (liquid + vapor) fluid inclusions in kyanite. Sample: ky-3

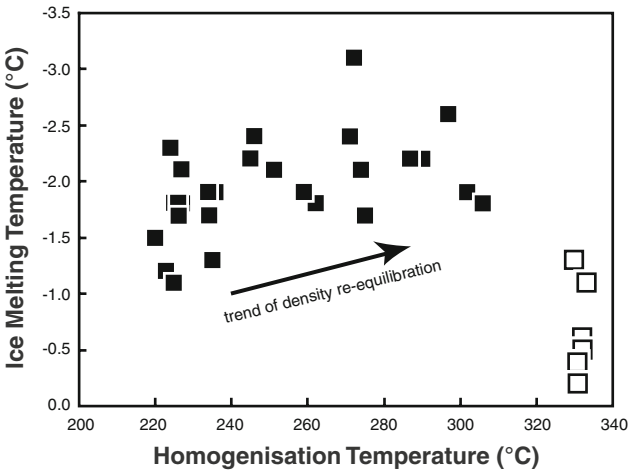

Fig. 8 Plot of homogenization (T_h) versus final ice melting (T_m) temperature of 34 kyanite-hosted fluid inclusions. Analytical uncertainty is indicated by the symbol size. *Filled symbols* represent pseudo-secondary fluid inclusions, whereas fluid inclusions shown by *open symbols* are either pseudo-secondary or secondary in origin

Thermodynamic modeling of Al transport

The textural observations, coupled with information from fluid inclusions, stable isotopes and geothermobarometry, indicate that fluid-assisted transport of Al and Si was essential in the formation of the quartz–kyanite veins and kyanite–mica lenses. Because both advective and diffusive processes have been discussed as important mechanisms resulting in mobility and transport of Al in regional metamorphic environments, we have applied thermodynamic modeling to evaluate Al solubility and complexing in amphibolite–facies aqueous fluids. In particular, this modeling involved assessment of the role of mixed Al–Si complexes in metamorphic fluids.

Thermodynamic model

Thermodynamic modeling has included calculation of predominance diagrams of aqueous Al complexes, speciation and solubility calculations, and reaction–path simulations of heterogeneous fluid–mineral equilibria in the model system Na–K–Al–Si–O–H–Cl–F–B. All calculations were done with the HCh software package (Shvarov and Bastrakov 1999), which models heterogeneous equilibria and reaction progress by minimization of the Gibbs free energy of the total system (Shvarov 1978, 1981). The thermodynamic data for pure mineral phases were taken from the internally consistent database of Holland and Powell (1998). Standard state thermodynamic properties of

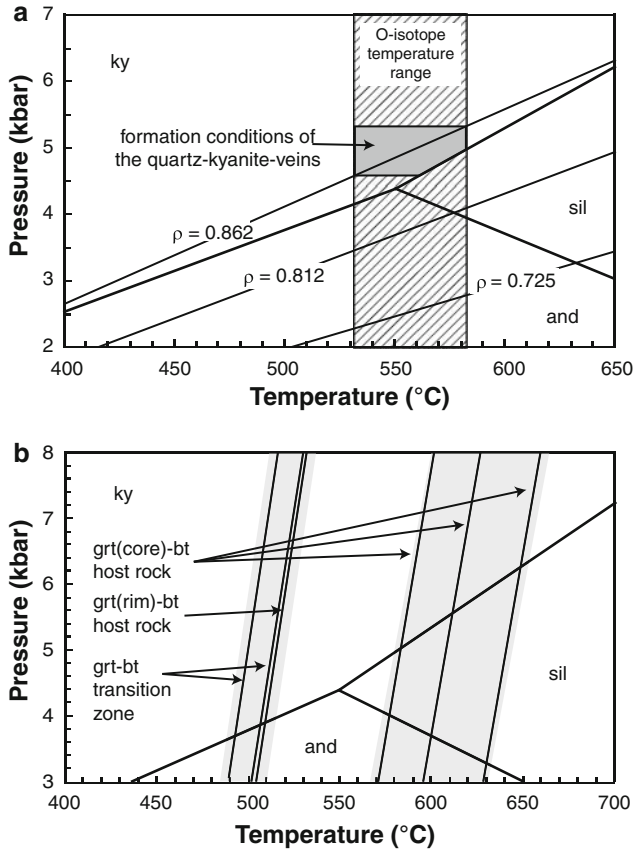

Fig. 9 **a** P–T-diagram with the isochores of three typical kyanite-hosted fluid inclusions (highest, intermediate, and lowest density). Also shown are the range in oxygen isotope equilibrium temperatures (calculated with the calibration of Richter and Hoernes 1988) obtained from texturally coexisting quartz–kyanite pairs, and the resulting formation conditions of the quartz–kyanite veins. **b** P–T-diagram with conditions obtained from garnet–biotite thermobarometry (Holdaway 2000). The alumosilicate stability fields (White et al. 2007) are shown in both diagrams

aqueous species at elevated temperatures and pressures were generally calculated from the modified Helgeson–Kirkham–Flowers (HKF) model (Tanger and Helgeson 1988; Shock et al. 1992). Individual aqueous species activity coefficients were calculated with an extended Debye–Hückel model, where the extended term is a function of temperature and pressure (Oelkers and Helgeson 1990). The thermodynamic data for most aqueous ions and complexes were taken from the SUPCRT92 database (Johnson et al. 1992; Shock et al. 1997; Sverjensky et al. 1997). This dataset has been augmented by critically evaluated data for aqueous Al species (Pokrovskii and Helgeson 1997; Tagirov and Schott 2001) and by recent reevaluation of the dissociation constant of aqueous HCl (Tagirov et al. 1997).

The published databases and compilations contain thermodynamic data for a considerable number of aqueous Al species, but no data are available for Al–Si and Al–B complexes (except $AlH_3SiO_4^{2+}$ that is only important at acid pH conditions), that are expected to be important species in Si- and B-rich aqueous fluids at elevated temperatures and pressures (Pokrovski et al. 1998; Tagirov et al. 2002, 2004; Manning 2007). Therefore, we derived equation of state parameters from experimental data on the stability of the two important complexes $AlSi(OH)_6O^-$ (Pokrovski et al. 1998) and $AlB(OH)_5O^-$ (Tagirov et al. 2004). We used the hydrated stoichiometry for the species $AlSi(OH)_6O^-$. This is formally identical to $AlSiO_4^-$, which has been discussed as one potential candidate responsible for Al–Si complexing in high-pressure fluids (Manning 2007). Because only four equilibrium constants were available for the two complexes $AlSi(OH)_6O^-$ and $AlB(OH)_5O^-$, it was not possible to refine a set of HKF parameters. Therefore, we have resorted to the modified Ryzhenko–Bryzgalin (MRB) model (Shvarov and Bastrakov 1999) instead, which requires fewer experimental data for calibration. A comprehensive description of this model is given in the appendix. The MRB model yields a reasonable representation of complex formation constants up to about 600°C and 5 kbar (Shvarov and Bastrakov 1999). A complete list of our aqueous Al speciation scheme is given in Table 4.

The validity of the Al speciation model has been carefully tested by comparison of calculated corundum and quartz solubilities (in pure water) with experimentally determined values (Tropper and Manning 2007; Manning 1994). The agreement in the temperature range 500–600°C and pressures of 3–5 kbar is good (Fig. 10). Comparison with experimental quartz–kyanite solubilities at metamorphic P–T conditions was not possible, because the experiments of Manning (2007) were conducted at a pressure of 10 kbar, well outside the limits of applicability of the HKF and MRB equations of state (Johnson et al. 1992).

Stability relationships of aqueous Al complexes

We have calculated a series of predominance diagrams for aqueous species in the system Na–K–Al–Si–O–H–Cl–F–B, in order to identify the most important species involved in aluminum transport and to constrain the effects of bulk fluid salinity and of additional ligands such as F, B and SiO_2 in the fluid. All diagrams were computed for constant P–T conditions of 5 kbar and 500°C (Fig. 11). Because the aqueous Al speciation is strongly dependent on pH, we fixed pH at neutral in those diagrams where pH is not a variable (4.4 at 500°C and 5 kbar, from the ion product of water, Marshall and Franck 1981). The results of our calculations show that the control of K and B concentrations on aqueous Al speciation appears to be insignificant for

Table 4 Overview of aqueous Al species considered in the thermodynamic modeling, with equations of state used and respective data sources

Species	Model	Data source
Al^{3+}	HKF	Tagirov and Schott (2001)
$AlOH^{2+}$	HKF	Tagirov and Schott (2001)
$Al(OH)_2^+$	HKF	Tagirov and Schott (2001)
$Al(OH)_3$	HKF	Tagirov and Schott (2001)
$Al(OH)_4^-$	HKF	Tagirov and Schott (2001)
AlF^{2+}	HKF	Tagirov and Schott (2001)
AlF_2^+	HKF	Tagirov and Schott (2001)
AlF_3	HKF	Tagirov and Schott (2001)
AlF_4^-	HKF	Tagirov and Schott (2001)
$AlOHF_2$	HKF	Tagirov and Schott (2001)
$Al(OH)_2F$	HKF	Tagirov and Schott (2001)
$Al(OH)_2F_2^-$	HKF	Tagirov and Schott (2001)
$NaAl(OH)_4$	HKF	Tagirov and Schott (2001)
$NaAl(OH)_3F$	HKF	Tagirov and Schott (2001)
$NaAl(OH)_2F_2$	HKF	Tagirov and Schott (2001)
$AlH_3SiO_4^{2+}$	HKF	Tagirov and Schott (2001)
$AlSi(OH)_6O^-$	MRB	Pokrovski et al.(1998)
$KAlO_2$	HKF	Pokrovskii and Helgeson (1997)
$AlB(OH)_5O^-$	MRB	Tagirov et al. (2004)

HKF modified Helgeson–Kirkham–Flowers model (Tanger and Helgeson 1988), *MRB* modified Ryzhenko–Bryzgalin model (Shvarov and Bastrakov 1999

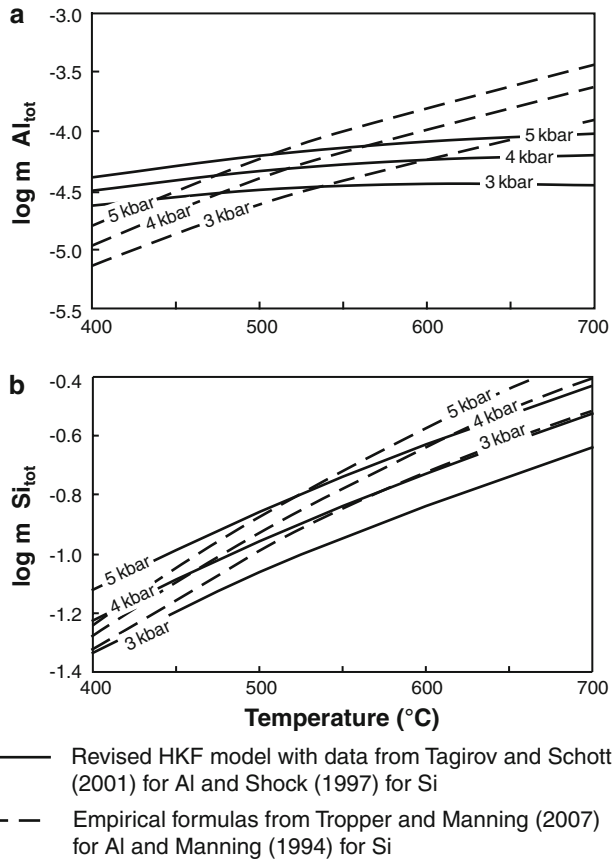

Fig. 10 Comparison of the calculated (*solid lines*) corundum (**a**) and quartz (**b**) solubility in pure water with experimentally determined (*dashed lines*) solubilities (Tropper and Manning 2007; Manning 1994). The speciation scheme employed for the solubility calculations included Al^{3+} and Al hydroxide complexes for modeling corundum and SiO_2 (aq) for quartz solubility. Pressure and temperature corrections were done with the revised HKF equation of state (Tanger and Helgeson 1988) and parameters given in Shock et al. (1997) and Tagirov and Schott (2001)

geologically reasonable conditions (not illustrated in Fig. 11). The concentration of boron would have to exceed 3 wt.% in the fluid to exert a detectable influence on the Al speciation. Similarly, the K concentration would have to be equal to the Na concentration for K aluminate species to become important. This differs from experimentally determined K/Na ratios of 0.33–0.34 in aqueous fluids in equilibrium with average metapelites in the temperature interval 600–650°C (Hauzenberger et al. 2001; Pak et al. 2003). With decreasing temperature, the K/Na ratios in metamorphic fluids are expected to further decrease (Orville 1963; Hauzenberger et al. 2001).

Consequently, aqueous Al speciation in typical amphibolite–facies metamorphic fluids is dominantly controlled by bulk salinity (as expressed by the Na^+ activity) and the concentrations of fluorine and aqueous silica. This is because mixed Na–Al–OH–F complexes can be important over a wide range in Na^+ and F^- activities (Fig. 11a) at neutral pH conditions, whereas mixed Al–Si complexes become predominant at aqueous silica activities that are achieved in metamorphic fluids saturated with quartz (Fig. 11b). In quartz-saturated metamorphic fluids, the relative abundance of mixed Al–Si complexes would be always greater than that of Al hydroxide species. At low pH values well below the neutral point, the species $AlH_3SiO_4^{2+}$ would predominate, whereas at slightly acidic to strongly alkaline pH the species $AlSi(OH)_6O^-$ would be dominant (Fig. 11b).

Mineral solubility and reaction–path modeling

Previous studies (e.g., Verlaguet et al. 2006) have shown that the amount of aluminum that can be transported in a metamorphic fluid using only Al hydroxide complexes is generally not sufficient to form the quartz–kyanite veins observed. Calculations applying simple empirical equations for Al (Tropper and Manning 2007) and SiO_2 (Manning 1994) solubility in metamorphic fluids predict a vein assemblage with 0.07 vol.% kyanite for isobaric cooling in the temperature range 600–500°C at 5 kbar.

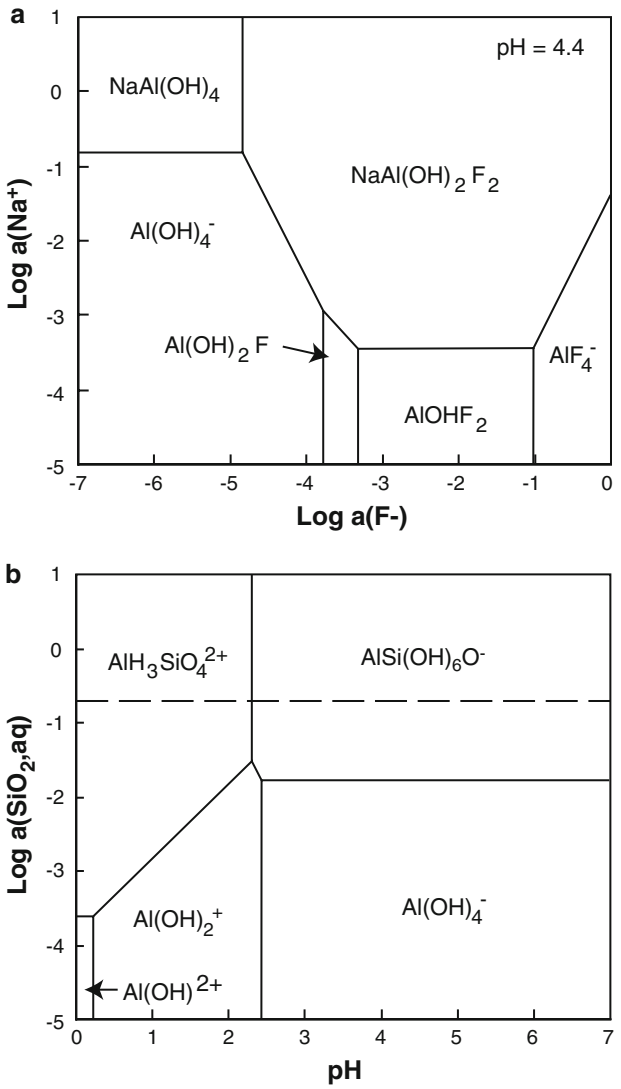

Fig. 11 Predominance diagrams of aqueous Al species in the system Na–Al–Si–O–H–F calculated at 500°C and 5 kbar. **a** Stability of Al complexes as a function of the activity of Na^+ and F^-. The pH has been fixed at the neutral value of 4.4, which was calculated from the water dissociation constant given by Marshall and Franck (1981). **b** Stability of Al complexes as a function of the SiO_2 (aq) activity and pH. For this diagram, Na and F have not been considered. The quartz saturation boundary is shown as a *dashed line*

This is much less kyanite than the proportion observed in the veins of the Alpe Sponda and more complex Al speciation models have to be considered.

We therefore have included Al–Si, Al–F, Al–Na, Al–K and Al–B complexing into our solubility model. We have calculated the pH-dependent kyanite solubility in the temperature interval 600–500°C at a constant pressure of 5 kbar with two model fluid compositions, one with very low concentrations of F and Na and the other with higher concentrations of both elements. It is noted that the concentration of Na in metamorphic fluids is mainly controlled by the halite saturation limit and Na–K exchange equilibria with feldspar and mica assemblages. By contrast, the concentration of F in aqueous fluids will be essentially controlled by fluorite saturation, which is dependent on the given Ca concentration in the fluid. If the fluid has low Ca concentrations, the corresponding F concentrations can be substantial, whereas in a more Ca-rich fluid fluorite saturation will effectively buffer the F level at much lower values. In order to account for these chemical effects, we have to a first approximation considered the concentration ranges that have been reported in the literature (Bottrell and Yardley 1988; Tagirov and Schott 2001) and constructed two model fluids that are assumed to represent end-member compositions. For both model fluids, the K/Na ratio was kept constant (0.3 in weight units) and the concentration of $B(OH)_3$ was set to a value of 100 ppm that was considered typical for metamorphic fluids (Yardley and Shmulovich 1994). It is noted that the concentration of boric acid in the fluid would have to exceed 3 wt.% in order to significantly influence the solubility of Al. Such high concentrations of $B(OH)_3$ appear to be highly unlikely, considering reported boron concentrations in diverse types of crustal fluids (e.g., Prokofev et al. 2002). In addition, we have assumed that the fluid is always at quartz saturation. The results of these comprehensive speciation calculations indicate significantly higher kyanite solubilities than predicted with the simple empirical equations that are based on Al hydroxide complexing alone (Tropper and Manning 2007).

We have then modeled the simultaneous precipitation of quartz and kyanite for isobaric cooling in the temperature range 600–500°C (at neutral pH) for both fluid compositions. The fluid that has low salinity and low F concentration reaches the maximum Al solubility at the point where it is in equilibrium with both quartz and kyanite (Fig. 12). The dominant aqueous silica species is still SiO_2 (aq), and silica solubility is only slightly enhanced by the formation of mixed Al–Si and Na–Si complexes. During cooling, the fluid remains in equilibrium with quartz and kyanite that are precipitated without requiring any chemical effects through interaction with the host–rock gneisses. Fluid cooling in the temperature range 600–500°C would then result in precipitation of quartz–kyanite assemblages with approximately 1.3 vol.% kyanite, which agrees nicely with the proportion of kyanite that is observed in the veins of the Alpe Sponda. Taking into account an additional pressure decrease from 5 to 4 kbar would result in a slight decrease of the amount of kyanite to 1.15 vol.%, demonstrating that pressure effects were not of major importance.

These simple solubility calculations are supported by reaction–path modeling that was designed to simulate both reversible and irreversible fluid cooling paths. In the reversible simulations, re-equilibration of the precipitated

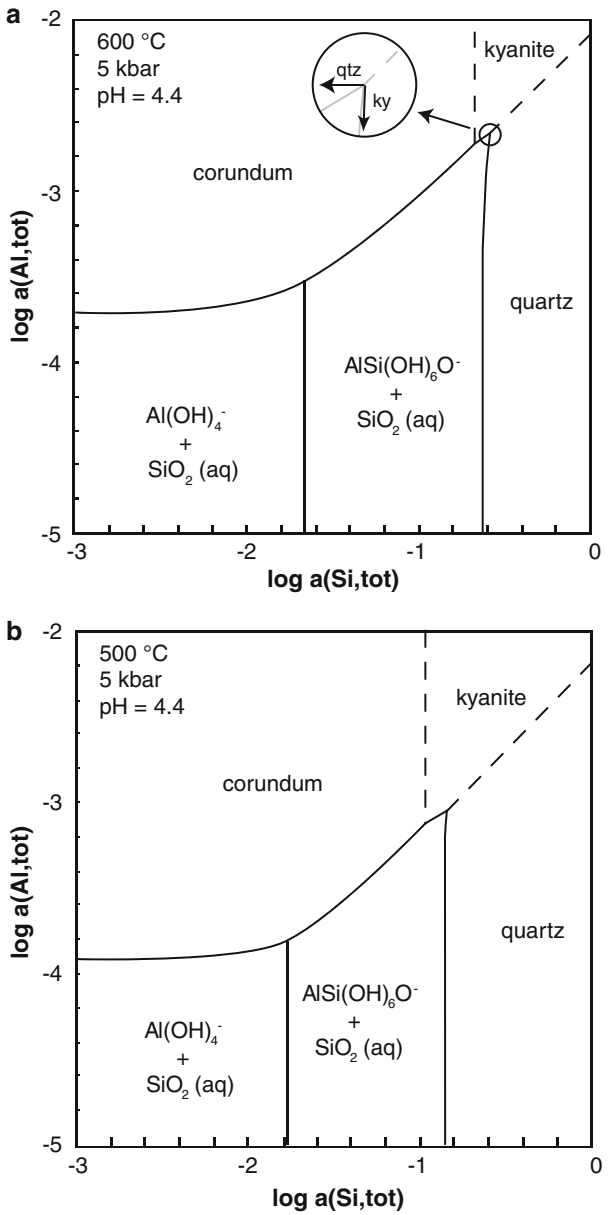

Fig. 12 Solubility diagrams dependent on Al and Si activities at 600 and 500°C at otherwise constant conditions (5 kbar and neutral pH) of a fluid poor in Na and F. The variables a(Al,tot) and a(Si,tot) that are plotted represent the sum of the activities of all aqueous Al and Si species, respectively. The *circle* shows the precipitation vectors for kyanite and quartz at the start of the modeled path at 600°C and SiO_2 (aq) and Al-saturation. *Thick solid lines* represent equilibrium of the fluid with the solid phase, *thin solid lines* the predominance fields of the Al complexes, and *dashed lines* metastable, unrealizable phase transitions. The topology of the diagrams agrees with that found experimentally at conditions of 700°C and 10 kbar (Manning 2007)

mineral assemblage with the fluid was allowed for each step, whereas in irreversible simulations the fluid was removed from the precipitated minerals and then allowed to cool for another small temperature increment. In these simulations, the starting fluids had a bulk salinity of 3.2 wt.% eqv. NaCl (the mean value obtained from the fluid inclusion studies) and a molar K/Na ratio of 0.33 that is typical for fluids in equilibrium with metapelites (Hauzenberger et al. 2001). This fluid was equilibrated with alumosilicate + quartz at starting temperatures of 600, 650, and 700°C and a pressure of 5 kbar. The pH was then adjusted to the neutral value at the respective P–T conditions. Then, the fluids were cooled down to 400°C in steps of 5°C (Fig. 13). The results of the simulations show that fluids that were saturated with alumosilicate + quartz at 700°C will precipitate kyanite + quartz down to 400°C, whereas fluids having a starting temperature of 650 and 600°C will start to precipitate muscovite instead of alumosilicates at about 550 and 570°C, respectively (Fig. 13a). The reaction–path simulations predict a kyanite proportion in the range of 3.6–5.2 vol.%, slightly higher than the simple solubility model described above. This represents even more closely the observed average proportion of kyanite in the veins.

Using mass balance relationships, we were able to calculate the amount of fluid required to transport the calculated amounts of aluminum and silica. From the reaction–path simulations, the fluid/rock ratio (by mass) for each cooling increment could be calculated (Fig. 14). Note that we use the (time-integrated) fluid/rock ratio as a proxy for the amount of fluid that is required to precipitate a given amount of vein filling, but not to indicate an instantaneous fluid/rock ratio that would correspond to a saturated porosity. For the first small cooling increment of 5°C, the fluid/rock ratio is calculated as about 2,920 (by mass). Along the reversible mineral precipitation path, the fluid/rock ratio decreases down to a value of 105 for a maximum temperature difference of 100°C (considering the maximum range in vein formation temperatures obtained from the geothermometric estimates). Calculated fluid/rock ratios in the irreversible simulation increase with reaction progress and reach a maximum value of about 6,040.

It is estimated that thermal gradients along fluid flow paths such as the kyanite–quartz vein systems would be on the order of not more than 10–30°C. Therefore, fluid/rock ratios would have to be larger than 510, the value obtained for a 30°C gradient in the reversible path. Using a fluid density of 0.88 g cm^{-3}, this value would correspond to a volumetric fluid/rock ratio of 1,540. Compared to previous work that estimated the time-integrated volumetric fluid/rock ratio of unveined metapelites as up to 1,000 (Wood and Walther 1986), our calculated fluid amounts are only larger by a factor of 1.5–9.7, depending on the chosen gradient and the simulation path. Considering that the quartz–kyanite veins of the Alpe Sponda were formed in a structural setting that would favor substantial advective

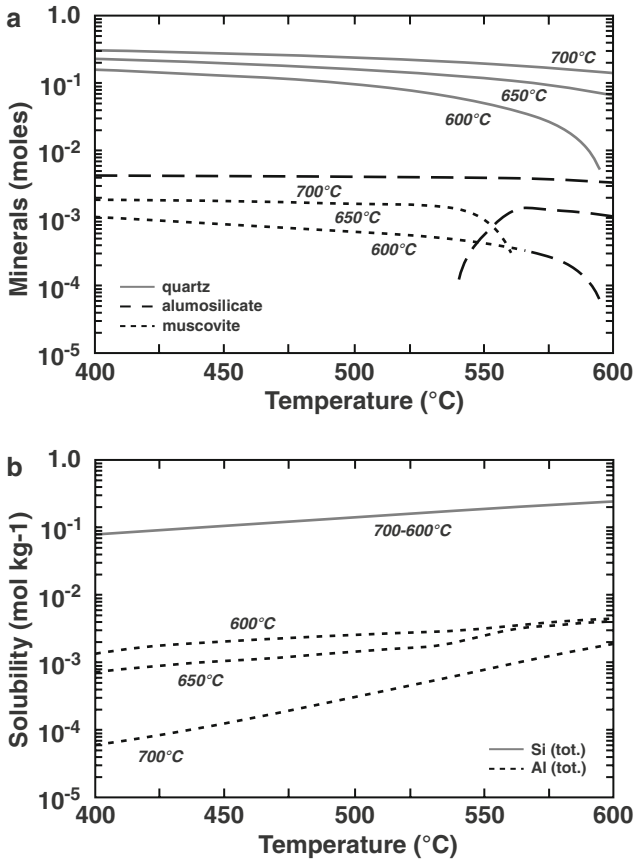

Fig. 13 Results of reaction–path modeling in the model system Na–K–Al–Si–Cl–O–H, showing the effect of cooling aqueous metamorphic fluids saturated with quartz + alumosilicate. Three simulations have been performed, with starting temperatures of 600, 650 and 700°C. Shown are (**a**) temperature effect on cumulative (reversible) precipitation of minerals, and (**b**) corresponding total Si and Al solubility in the model fluid. In the temperature interval 600–550°C, significant amounts of quartz + alumosilicate assemblages will precipitate from fluids that were saturated with this assemblage above 650°C, whereas fluids that achieved saturation at lower temperatures will precipitate quartz + muscovite below about 550–560°C

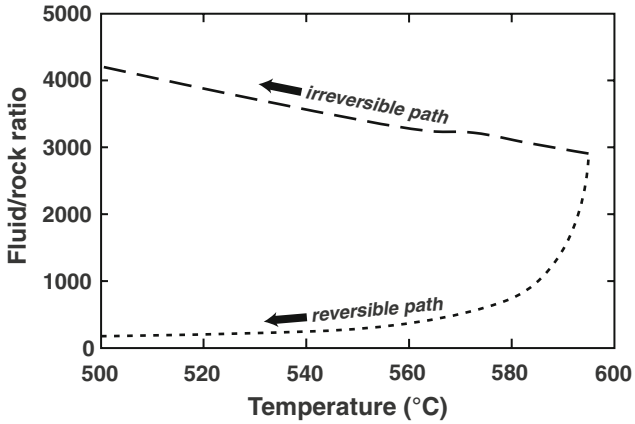

Fig. 14 Calculated fluid/rock ratios (equivalent to fluid amounts required for precipitation of a given amount of vein filling) for two different reaction path simulations, where a fluid in equilibrium with a kyanite + quartz assemblage was allowed to cool from 600°C down to 500°C. In the reversible path simulation the fluid was cooled from 600°C in one step to each temperature. The fluid/rock ratio was then obtained from the given amount of fluid and the total amount of solids that precipitated. In the irreversible simulation, the fluid was cooled in small increments of 5°C and the minerals that precipitated were left behind in the subsequent cooling step. The fluid/rock ratio was then calculated for each cooling increment. The calculated fluid amounts can be compared to estimates of typical fluid fluxes in metamorphic terranes (e.g., Wood and Walther 1986; Wing and Ferry 2007)

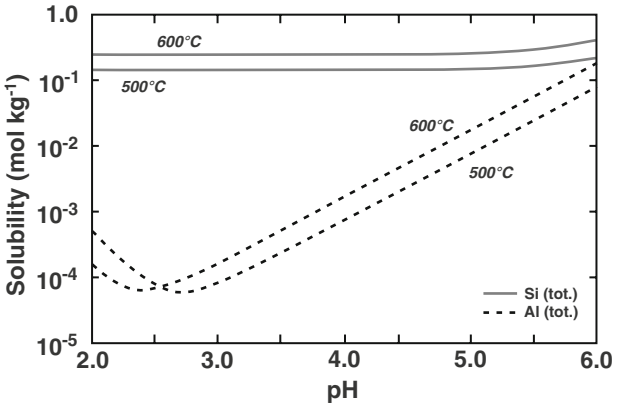

Fig. 15 Calculated total solubility of aluminum and silica in a fluid in equilibrium with a kyanite–quartz assemblage as function of pH. The solubility has been calculated at both 600 and 500°C. The aluminum solubility has a pronounced minimum at slighly acid pH (neutral pH is about 4.4 in the temperature interval 600–500°C) that shifts to a higher value with decreasing temperature

fluid flow, we conclude that sufficient aluminum can be transported in typical amphibolite–facies metamorphic fluids involving reasonable fluid fluxes. Furthermore, our calculations demonstrate that it is not necessary to involve additional processes such as diffusion-controlled local derivation of material to explain the vein formation.

In addition to temperature changes, variations in pH could also favor precipitation of kyanite-bearing assemblages. To test the effect of pH, we have calculated the solubility of quartz + kyanite as a function of pH, both at 600 and 500°C. The results of our modeling show that the solubility of aluminum is strongly dependent on pH (Fig. 15), with a pronounced solubility minimum occurring at slightly acidic pH (neutral pH is about 4.4 in the temperature interval 600–500°C; Marshall and Franck 1981). It is noted that the solubility minimum shifts by about 0.5 pH units with temperature decreasing from 600 to 500°C. The topology of the calculated solubility diagram suggests that fluids that are more acidic than the solubility minimum would precipitate alumosilicate minerals upon reaction with rock assemblages that would buffer pH at more alkaline conditions.

Conversely, a fluid that was initially equilibrated with a rock assemblage that would buffer pH at conditions more

alkaline than the solubility minimum would precipitate an aluminum phase upon decrease of pH. Such a process would be likely for a fluid that would cool under fluid-buffered conditions (i.e., without re-equilibration with wall rock assemblages). This is because the general increase in dielectrical constant of the water solvent with decreasing temperature would promote substantial dissociation of HCl^0 and production of H^+ ions (e.g., Tagirov et al. 1997; Dolejs and Wagner 2008). Therefore, fluid cooling along even a small temperature gradient would likely result in precipitation of quartz–kyanite assemblages through the enhancing effects of temperature dependent solubility decrease and fluid pH decrease.

Discussion and conclusions

The textural observations, fluid inclusion information and stable isotope data, coupled with the results of thermodynamic modeling, demonstrate that significant amounts of aluminum were transported in regional metamorphic fluids that formed the quartz–kyanite veins of the Alpe Sponda. The results of our study support conclusions drawn from field-based and experimental studies, which have suggested that aluminum will behave rather mobile in medium- to high-grade metamorphic rocks (Kerrick 1988; Manning 1998, 2006; Widmer and Thompson 2001). This result is in contrast to earlier studies that assumed that aluminum is relatively immobile during fluid–rock interaction (Carmichael 1969; Thompson 1975; Ragnarsdottir and Walther 1985; Grant 1986; Ferry 1987, 1988). Remarkably, our solubility and reaction–path calculations are able to predict both the mineral assemblage and the mineral proportions observed in the quartz–kyanite veins of the Alpe Sponda. The excellent agreement between model prediction and field observation strongly substantiates our conceptual model, where simple fluid cooling along a small temperature gradient (coupled with pH decrease) is the major mechanism responsible for vein formation. It appears likely that this model can be applied to other regionally metamorphosed terranes, where quartz–kyanite veins with comparatively low proportions of kyanite (less than about 10 vol.%) have been observed (Klein 1976; Franz et al. 2001).

Strong Al–Si complexing in amphibolite-grade metamorphic fluids, as previously proposed based on experimental solubilities of the kyanite + quartz assemblage (Manning 2007), is the essential factor that controls transport and mobility of aluminum. Because typical aqueous metamorphic fluids that originate from regional devolatilization are generally close to quartz saturation (Manning 1994; Newton and Manning 2003), the Al concentrations are mainly controlled by the temperature-dependent silica solubility (Walther and Helgeson 1977; Xie and Walther 1993). In addition, fluid pH exerts another important control on the solubility of the kyanite–quartz assemblage through the reaction:

$$Al_2SiO_5(ky) + SiO_2(qz) + 7H_2O = 2AlSi(OH)_6O^- + 2H^+ \quad (1)$$

Decrease in pH through reactions with rock lithologies that would buffer pH at a value lower than fluid pH or a pH decrease through HCl^0 dissociation upon fluid cooling would then result in precipitation of quartz–kyanite assemblages. Only if the metamorphic fluids have exceptionally high salinities, as is the case with some fluids that originate from granulite facies terranes (Clemens and Droop 1998) or from fluid systems that experienced significant input of magmatic brines (Frank et al. 2003), alkali–Al complexes will become more important than Al–Si species.

It has to be noted that the above conclusions about the effect of fluid salinity and pH on Al solubility are strongly dependent on the chosen aqueous speciation model. Manning (2007) has assumed that the neutral species $AlSi(OH)_5O$ would be the predominant Si–Al complex at high temperatures and pressures. Because the experiments of Manning (2007) were only performed at one state point (700°C, 10 kbar), it is currently not possible to extract thermodynamic information that would allow to include the $AlSi(OH)_5O$ complex into a comprehensive speciation model. If this complex would strongly dominate over $AlSi(OH)_6O^-$ that we have considered in our study, the solubility of kyanite + quartz would become pH independent:

$$Al_2SiO_5(ky) + SiO_2(qz) + 5H_2O = 2AlSi(OH)_5O \quad (2)$$

with the current experimental information, it is not possible to decide if $AlSi(OH)_6O^-$ or $AlSi(OH)_5O$ will be the dominant Si–Al species at elevated temperatures and pressures. Although the strong decrease of the dielectrical constant of the water solvent with increasing temperature would strongly favor the formation of neutral species and ion pairs at temperatures above 300–400°C, the stabilizing effect of the tetrahedral Al–ligand coordination in solution that has been noted by Salvi et al. (1998) and Pokrovski et al. (1998) might be able to overcompensate this.

Newton and Manning (2007, 2008), based on experimental studies of the solubility of grossular and corundum in $NaCl–H_2O$ fluids, have convincingly argued that polymeric Na–Si–Al complexes will be significant at conditions of 800°C and 10 kbar. If complexes like $NaAlSi(OH)_6O$ (or its K equivalent) are the dominant Al species in saline fluids, the solubility of kyanite + quartz will become dependent on both salinity and pH:

$$Al_2SiO_5(ky) + SiO_2(qz) + 7H_2O + 2Na^+ = 2NaAlSi(OH)_6O + 2H^+ \quad (3)$$

For fluids having moderate to high salinity, this would lead to a significant solubility enhancement (Newton and Manning 2007, 2008), whereas for the low-salinity fluids that were involved in the quartz–kyanite veins of the Alpe Sponda, this effect would be relatively unimportant.

Although our model is able to explain the formation of quartz–kyanite veins in many regionally metamorphosed terranes, we note that alumosilicate veins that have very high proportions of aluminum minerals compared to the associated silicate and oxide minerals require the involvement of additional factors. Precipitation of very large proportions of aluminum minerals in such veins requires very high Al solubilities coupled with low solubilities of quartz and other silicate minerals. These chemical characteristics cannot be achieved by moderate deviations of the pH from the neutral value. The calculated predominance diagram in the Al–Si–O–H system shows that the speciation of Al changes only at very low pH values below about 2.5 (Fig. 11b). This implies that very low pH values are required for enhanced Al solubility at constant silica solubility, which is controlled by the neutral species SiO_2 (aq) and its polymers (Manning 1994; Newton and Manning 2003). Such low pH values are unlikely to be attained in aqueous fluids generated during regional metamorphism, because the ubiquitous presence of feldspar–white mica assemblages will buffer fluid pH at values close to neutral. Only if fluids evolve along fluid–buffered paths without re-equilibration with the surrounding rocks such low pH values can be achieved upon cooling and re-dissociation of HCl (Tagirov et al. 1997).

In fluids with more alkaline pH, the solubility of aluminum will systematically increase with pH, but this effect will be counterbalanced by the strong increase in silica solubility due to the formation of $HSiO_3^-$ and the ion pairs with Na, K, Mg and Ca (Sverjensky et al. 1997). Based on the above considerations, no obvious feasible mechanism for preferential Al solubility and transport in metamorphic fluids can be envisaged. It appears likely that formation of veins and segregations (such as the kyanite–mica lenses at the Alpe Sponda) in metamorphic rocks that are dominantly composed of alumosilicate minerals require processes such as preferential Al diffusion along chemical potential gradients (Widmer and Thompson 2001), preferential leaching of elements via fluid–rock interaction, or dissolution–reprecipitation reactions, which could be enhanced by deformation and grain size effects.

Acknowledgments We would like to thank Indra Gill–Kopp for preparation of thin and doubly polished sections, Thomas Wenzel for his help and support during electron-microprobe analysis, and Bernd Steinhilber and Heiner Taubald for assisting with the stable isotope analysis. The research of Gregor Markl and Thomas Wagner was supported by the Alfred Krupp Prize for Young University Teachers of the Krupp Foundation. We thank the two Contributions to Mineralogy and Petrology reviewers, Craig Manning and John Ferry, for their very detailed and constructive comments that have greatly improved our paper. Any remaining errors and omissions are solely our responsibility.

Appendix 1: The modified Ryzhenko–Bryzgalin (MRB) model for aqueous electrolytes

The modified Ryzhenko–Bryzgalin (MRB) model is based on electrostatic models that were developed to extrapolate formation constants of aqueous complexes to elevated temperatures and pressures. The original model formulation included an explicit dependence of the equilibrium constant (or pK, the negative logarithm of the equilibrium constant) on water density and dielectric constant (Ryzhenko et al. 1985; Bryzgalin 1986, 1989).

$$pK_{T,P} = pK_{298,1}\frac{298}{T} + \frac{e^2Nz^+z^-}{\ln(10)RTa}\left(\frac{1}{\varepsilon_{T,P}} - \frac{1}{\varepsilon_{298,1}}\right) \quad (A1-1)$$

Here, e is the electron charge, N is the Avogadro number, z^+ and z^- are the ionic charges, and ε is the dielectric constant of water at P and T of interest. The term a stands for the sum of the crystallographic radii of the ions. By comparing the model predictions with experimental data, it was found that the parameter a would differ from the sum of the crystallographic radii. Therefore, this parameter was combined with the ionic charges into the adjustable parameter (zz/a), similar to the effective electrostatic radii in the modified HKF model (Tanger and Helgeson 1988). From this, the new basic model equation would become (Shvarov and Bastrakov 1999).

$$pK_{T,P} = pK_{298,1}\frac{298}{T} + \bar{B}_{T,P}(zz/a) \quad (A1-2)$$

The parameter $\bar{B}_{T,P}$ does not depend on the complex type, but only on pressure and temperature. It would be calculated from the dissociation constant of water as given by Marshall and Franck (1981).

$$\log K^W_{T,P} = a + \frac{b}{T} + \frac{c}{T^2} + \frac{d}{T^3} + \left(e + \frac{f}{T} + \frac{g}{T^2}\right)\log\rho. \quad (A1-3)$$

This would result in a best-fit value of 1.0107 for $(zz/a)_W$ (Shvarov and Bastrakov 1999). The function $\bar{B}_{T,P}$ can then be calculated at any pressure and temperature. To improve the representation of experimentally determined complex

dissociation constants, the parameter (zz/a) would become temperature dependent (Shvarov and Bastrakov 1999).

$$(zz/a) = A + B/T \qquad (A1-4)$$

By noting the relationship between $\Delta_r G^{\circ}_{T,P}$ and the equilibrium constant

$$pK_{T,P} = \frac{\Delta_r G^{\circ}_{T,P}}{RT\ln(10)} \qquad (A1-5)$$

the full expression for the Gibbs free energy of reaction, $\Delta_r G^{\circ}_{T,P}$, can be obtained, and the properties of the aqueous complex are then calculated from the constituting basic ions by difference.

References

Addy SK, Garlick GD (1974) Oxygen isotope fractionation between rutile and water. Contrib Mineral Petrol 45:119–121

Armstrong JT (1991) Quantitative elemental analysis of individual microparticles with electron beam instruments. In: Heinrich KFJ, Newbury DE (eds) Electron probe quantitation. New York, pp 261–315

Bakker RJ (2003) Package FLUIDS 1 Computer programs for analysis of fluid inclusion data and for modelling bulk fluid properties. Chem Geol 194:3–23. doi:10.1016/S0009-2541(02) 00268-1

Blencoe JG, Guidotti CV, Sassi FP (1994) The paragonite–muscovite solvus. II. Numerical geothermometers for natural, quasibinary paragonite–muscovite pairs. Geochim Cosmochim Acta 58:2277–2288. doi:10.1016/0016-7037(94) 90010-8

Bodnar RJ, Vityk MO (1994) Interpretation of microthermometric data for H_2O–NaCl fluid inclusions. In: De Vivo B, Frezzotti ML (eds) Fluid inclusions in minerals, methods and applications. Blacksburg, pp 117–130

Bottrell SH, Yardley BWD (1988) The composition of a primary granite-derived ore fluid from S·W. England, determined by fluid inclusion analysis. Geochim Cosmochim Acta 52:585–588. doi: 10.1016/0016-7037(88) 90114-7

Bryzgalin OV (1986) Estimating dissociation constants in the supercritical region for some strong electrolytes from an electrostatic model. Geochem Int 23(2):84–95

Bryzgalin OV (1989) Electrostatic-model estimate of electrolyte dissociation constants up to 800°C and 5 kbar. Geochem Int 26(10):63–70

Carmichael DM (1969) On the mechanism of prograde metamorphic reactions in quartz bearing pelitic rocks. Contrib Mineral Petrol 20:244–267. doi:10.1007/BF00377479

Chacko T, Hu X, Mayeda TK, Clayton RN, Goldsmith JR (1996) Oxygen isotope fractionations in muscovite, phlogopite, and rutile. Geochim Cosmochim Acta 60:2595–2608. doi: 10.1016/0016-7037(96) 00112-3

Chatterjee ND, Flux S (1986) Thermodynamic mixing properties of muscovite–paragonite, crystalline solutions at high temperatures and pressures, and their geological applications. J Petrol 27:677–693

Clemens JD, Droop GTR (1998) Fluids, P–T paths and the fates of anatectic melts in the Earth's crust. Lithos 44:21–36. doi: 10.1016/S0024-4937(98) 00020-6

Diakonov I, Pokrovski G, Schott J, Castet S, Grout R (1996) An experimental and computational study of sodium–aluminum complexing in crustal fluids. Geochim Cosmochim Acta 60:197–211. doi:10.1016/0016-7037(95) 00403-3

Dolejs D, Wagner T (2008) Thermodynamic modeling of non-ideal mineral–fluid equilibria in the system Si–Al–Fe–Mg–Ca–Na–K–H–O–Cl at elevated temperatures and pressures: implications for hydrothermal mass transfer in granitic rocks. Geochim Cosmochim Acta 72:526–553. doi:10.1016/j.gca.2007.10.022

Ferry JM (1987) Metamorphic hydrology at 13-km depth and 400–500°C. Am Mineral 72:39–58

Ferry JM (1988) Contrasting mechanisms of fluid flow through adjacent stratigraphic units during regional metamorphism, south-central Maine, USA. Contrib Mineral Petrol 98:1–12. doi: 10.1007/BF00371903

Frank MR, Candela PA, Piccoli PM (2003) Alkali exchange equilibria between silicate melt and coexisting magmatic volatile phases: an experimental study at 800°C and 100 MPa. Geochim Cosmochim Acta 7:1415–1427. doi:10.1016/S0016-7037 (02) 01181-X

Franz L, Romer RL, Klemd R, Schmid R, Oberhänsli R, Wagner T et al (2001) Eclogite–facies quartz veins within metabasitesof the Dabie Shan (eastern China): pressure–temperature–time–deformation path, composition of the fluid phase and fluid flow during exhumationof high-pressure rocks. Contrib Mineral Petrol 141:322–346

Frey M, Mählmann RF (1999) Alpine metamorphism of the Central Alps. Schweiz Mineral Petrogr Mitt 79:135–154

Frisch W (1979) Tectonic progradation and plate tectonic evolution of the Alps. Tectonophysics 60:121–139. doi:10.1016/0040-1951 (79) 90155-0

Frisch W, Meschede M (2005) Plattentektonik. Wissenschaftlische Buchgesellschaft, Darmstadt

Gebauer D (1999) Alpine geochronology of the Central and Western Alps: new constraints for a complex geodynamic evolution. Schweiz Mineral Petrogr Mitt 79:191–208

Grant JA (1986) The isocon diagram—a simple solution to Gresens'equation for metasomatic alteration. Econ Geol 81:1976–1982

Hauzenberger CA, Baumgartner LP, Pak TM (2001) Experimental study on the solubility of the "model"-pelite mineral assemblage albite, K-feldspar, andalusite and quartz in supercritical chloride-rich solutions at 0.2 GPa and 600°C. Geochim Cosmochim Acta 65:4493–4507. doi:10.1016/S0016-7037(01)00741-4

Hoffbauer R, Hoernes S, Fiorentini E (1994) Oxygen isotope thermometry based on a refined increment method and its application to granulite–grade rocks from Sri Lanka. Prec Res 66:199–220. doi:10.1016/0301-9268(94) 90051-5

Holdaway MJ (2000) Application of new experimental and garnet Margules data to the garnet–biotite geothermometer. Am Mineral 85:881–892

Holland TJB, Powell R (1998) An internally consistent thermodynamic data set for phases of petrological interest. J Metamorph Geol 16:309–343. doi:10.1111/j.1525-1314.1998.00140.x

Irouschek A (1983) Mineralogie und Petrographie von Metapeliten der Simano-Decke unter besonderer Berücksichtigung cordieritführender Gesteine zwischen Alpe Sponda und Biasca. Ph.D. dissertation, Universität Basel, Schweiz.

Johnson JW, Oelkers EH, Helgeson HC (1992) SUPCRT92; a software package for calculating the standard molal thermodynamic properties of minerals, gases aqueous species, and reactions from 1 to 5000 bar and 0 to 1000 degree C. Comput Geosci 18:899–947. doi:10.1016/0098-3004(92) 90029-Q

Kelepertsis AE, Esson J (1987) Major- and trace-element mobility in altered volcanic rocks near Stypsi, Lesbos, Greece and genesis of a kaolin deposit. Appl Clay Sci 2:11–28. doi:10.1016/0169-1317(87) 90011-1

Keller F (1968) Mineralparagenesen und Geologie der Campo Tencia—Pizzo Forno—Gebirgsgruppe. Geographischer Verlag, Bern.

Kerrick DM (1988) Al_2SiO_5-bearing segregations in the Lepontine Alps, Switzerland: aluminum mobility in metapelites. Geology 16:636–640. doi:10.1130/0091-7613(1988) 016 ≤ 0636:ASBSIT ≥ 2.3.CO;2

Klein HH (1976) Alumosilikatführende Knauern im Lepontin. Schweiz Mineral Petrogr Mitt 56:435–456

Knight CL, Bodnar RJ (1989) Synthetic fluid inclusions: IX. Critical PVTX properties of NaCl–H_2O solutions. Geochim Cosmochim Acta 53:3–8. doi:10.1016/0016-7037(89)90267-6

Lentz DR, Gregoire C (1995) Petrology and mass-balance constraints on major-, trace- and rare-earth-element mobility in porphyry–greisen alteration associated with epizonal True Hill granite, south-western New Brunswick, Canada. J Geochem Explor 52:303–331. doi:10.1016/0375-6742(94) 00059-K

Manning CE (1994) The solubility of quartz in H_2O in the lower crust and upper mantle. Geochim Cosmochim Acta 58:4831–4839. doi:10.1016/0016-7037(94) 90214-3

Manning CE (1998) Fluid composition at the blueschist–eclogite transition in the model system Na_2O–MgO–Al_2O_3–SiO_2–H_2O–HCl. Schweiz Mineral Petrogr Mitt 78:225–242

Manning CE (2006) Mobilizing aluminum in crustal and mantle fluids. J Geochem Explor 89:251–253. doi:10.1016/j.gexplo.2005.12.019

Manning CE (2007) Solubility of corundum + kyanite in H_2O at 700°C and 10 kbar: evidence for Al–Si complexing at high pressure and temperature. Geofluids 7:258–269. doi:10.1111/j.1468-8123.2007.00179.x

Marshall WL, Franck EU (1981) Ion product of water substance, 0–1000°C, 1–10000 bars. New international formulation and its background. J Phys Chem Ref Data 10:295–304

Masters RL, Ague JJ (2005) Regional scale fluid flow and element mobility in Barrow's metamorphic zones, Stonehaven, Scotland. Contrib Mineral Petrol 150:1–18. doi:10.1007/s00410-005-0005-z

Matthews A (1994) Oxygen isotope geothermometers for metamorphic rocks. J Metam Geol 12:211–219

Maxelon M, Mancktelow NS (2005) Three-dimensional geometry and tectono-stratigraphy of the Pennine zone, Central Alps, Switzerland and Northern Italy. Earth Sci Rev 71:171–227. doi:10.1016/j.earscirev.2005.01.003

Milnes AG (1974) Structure of the Penninc Zone (Central Alps): a new working hypothesis. Geol Soc Am Bull 85:1727–1732. doi:10.1130/0016-7606(1974) 85 ≤ 1727:SOTPZC ≥ 2.0.CO;2

Newton RC, Manning CE (2003) Activity coefficient and polymerization of aqueous silica at 800°C, 12 kbar, from solubility measurements on SiO_2-buffered assemblages. Contrib Mineral Petrol 146:135–143. doi:10.1007/s00410-003-0483-9

Newton RC, Manning CE (2007) Solubility of grossulare, $Ca_3Al_2Si_3O1_2$, in H_2O–NaCl solutions at 800°C and 10kbar, and the stability of garnet in the system $CaSiO_3$–Al2O3–H_2O–NaCl. Geochim Cosmochim Acta 71:5191–5202. doi:10.1016/j.gca.2007.08.021

Newton RC, Manning CE (2008) Solubility of corundum in the system Al_2O_3–SiO_2–H_2O–NaCl at 800°C and 10 kbar. Chem Geol (in press)

Niggli E (1970) Alpine metamorphose und Gebirgsbildung. Fortschr Mineral 47:16–26

Oelkers EH, Helgeson HC (1990) Triple-ion anions and polynuclear compexing in supercritical electrolyte solutions. Geochim Cosmochim Acta 54:727–738. doi:10.1016/0016-7037(90) 90368-U

Orville PM (1963) Alkali ion exchange between vapor and feldspar phases. Am J Sci 261:201–239

Pak TM, Hauzenberger CA, Baumgartner LP (2003) Solubility of the assemblage albite + K-feldspar + andalusite + quartz in supercritical aqueous chloride solutions at 650°C and 2 kbar. Chem Geol 200:377–393. doi:10.1016/S0009-2541(03) 00211-0

Pokrovski GS, Schott J, Harrichoury JC, Sergeyev AS (1996) The stability of aluminum silicate complexes in acidic solutions from 25 to 150°C. Geochim Cosmochim Acta 60:2495–2501. doi:10.1016/0016-7037(96) 00123-8

Pokrovski GS, Schott J, Salvi S, Gout R, Kubicki JD (1998) Structure and stability of aluminium–silica complexes in neutral to basic solutions. Experimental study and molecular orbital calculations. Mineral Mag 62A:1194–1195. doi:10.1180/minmag.1998.62A.2.290

Pokrovskii VA, Helgeson HC (1995) Thermodynamic properties of aqueous species and the solubilities of minerals at high pressures and temperatures: the system Al_2O_3–H_2O–NaCl. Am J Sci 295:1255–1342

Pokrovskii VA, Helgeson HC (1997) Thermodynamic properties of aqueous species and the solubilities of minerals at high pressures and temperatures: the system Al_2O_3–H_2O–KOH. Chem Geol 137:221–242. doi:10.1016/S0009-2541(96) 00167-2

Prokofev VY, Akinfiev NN, Groznova EO (2002) On the boron concentration and forms of its occurrence in hydrothermal ore-forming fluids. Geol Ore Dep 44:386–397

Putlitz B, Valley JW, Matthews A, Katzir Y (2002) Oxygen isotope thermometry of quartz–Al_2SiO_5 veins in high-grade metamorphic rocks on Naxos Island (Greece). Contrib Mineral Petrol 143:350–359

Ragnarsdottir KV, Walther JV (1985) Experimental determination of corundum solubilities in pure water between 400–700°C and 1–3 kbars. Geochim Cosmochim Acta 49:2109–2115. doi:10.1016/0016-7037(85) 90068-7

Richter R, Hoernes S (1988) The application of the increment method in comparison with experimentally derived and calculated O-isotope fractionations. Chem Erde 48:1–18

Rubin JN, Henry CD, Price JG (1993) The mobility of zirconium and other "immobile"elements during hydrothermal alteration. Chem Geol 110:29–47. doi:10.1016/0009-2541(93) 90246-F

Rütti R (2003) The tectono-metamorphic evolution of the northwestern Simano Nappe (Central Alps, Switzerland). Ph.D. thesis, ETH Zürich

Rütti R, Maxelon M, Mancktelow NS (2005) Structure and kinematics of the northern Simano Nappe, Central Alps, Switzerland. Eclogae Geol Helv 98:63–81. doi:10.1007/s00015-005-1148-7

Ryzhenko BN, Bryzgalin OV, Artamkina IY, Spasennykh MY, Shapkin AI (1985) An electrostatic model for the electrolytic dissociation of inorganic substances dissolved in water. Geochem Int 22(9):138–144

Salvi S, Pokrovski GS, Schott J (1998) Experimental investigation of aluminum-silica aqueous complexing at 300°C. Chem Geol 151:51–67. doi:10.1016/S0009-2541(98) 00070-9

Sharp ZD (1992) In situ laser microprobe techniques for stable isotope analysis. Chem Geol 101:3–19

Sharp ZD (1995) Oxygen isotope geochemistry of the Al_2SiO_5 polymorphs. Am J Sci 295:1058–1076

Shock EL, Oelkers EH, Johnson JW, Sverjensky DA, Helgeson HC (1992) Calculation of the thermodynamic properties of aqueous species at high pressures and temperatures. Effective electrostatic radii, dissociation constants and standard partial molal properties to 1000°C and 5 kbar. J Chem Soc Faraday Trans 88:803–826. doi:10.1039/ft9928800803

Shock EL, Sassani DC, Willis M, Sverjensky DA (1997) Inorganic species in geological fluids: correlations among standard molal thermodynamic properties of aqueous ions and hydroxide complexes. Geochim Cosmochim Acta 61:907–950. doi:10.1016/S0016-7037(96) 00339-0 Medline

Shvarov YV (1978) Minimization of the thermodynamic potential of an open chemical system. Geochem Int 15:200–203

Shvarov YV (1981) A general equilibrium criterion for an isobaric–isothermal model of a chemical system. Geochem Int 18:38–45

Shvarov YV, Bastrakov E (1999) HCh: a software package for geochemical equilibrium modelling. User's guide. Australian Geological Survey Organisation. Science and Resources. Record 1999/25, 61 pp.

Sverjensky DA, Shock EL, Helgeson HC (1997) Prediction of the thermodynamic properties of aqueous metal complexes to 1000°C and 5 kb. Geochim Cosmochim Acta 61:1359–1412. doi:10.1016/S0016-7037(97) 00009-4 Medline

Sterner SM, Bodnar RJ (1989) Synthetic fluid inclusions-VII. Re-equilibration of fluid inclusions in quartz during laboratory-simulated metamorphic burial and uplift. J Metamorph Geol 7:243–260. doi:10.1111/j.1525-1314.1989.tb00587.x

Tagirov B, Zotov AV, Akinfiev NN (1997) Experimental study of dissociation of HCl from 350 to 500°C and from 500 to 2500 bars. Thermodynamic properties of HCl^0(aq). Geochim Cosmochim Acta 61:4267–4280. doi:10.1016/S0016-7037(97)00274-3

Tagirov B, Schott J (2001) Aluminum speciation in crustal fluids revisited. Geochim Cosmochim Acta 65:3965–3992. doi: 10.1016/S0016-7037(01) 00705-0

Tagirov B, Schott J, Harrichoury JC, Salvi S (2002) Experimental study of aluminium speciation in fluoride-rich supercritical fluids. Geochim Cosmochim Acta 66:2013–2024. doi: 10.1016/S0016-7037(01) 00899-7

Tagirov B, Schott J, Harrichoury JC, Escalier J (2004) Experimental study of the stability of aluminium–borate complexes in hydrothermal solutions. Geochim Cosmochim Acta 68:1333–1345. doi:10.1016/j.gca.2003.08.018

IV Tanger JC, Helgeson HC (1988) Calculation of the thermodynamic and transport properties of aqueous species at high pressures and temperatures: revised equations of state for the standard partial molal properties of ions and electrolytes. Am J Sci 288:19–98

Tennie A, Hoffbauer R, Hoernes S (1998) The oxygen isotope fractionation behaviour of kyanite in experiment and nature. Contrib Mineral Petrol 133:346–355. doi:10.1007/s004100050457

Thompson AB (1975) Calc–silicate diffusion zones between marble and politic schist. J Petrol 16:314–346

Todd CS, Engi M (1997) Metamorphic field gradients in the central Alps. J Metamorph Geol 15:513–530. doi:10.1111/j.1525-1314.1997.00038.x

Tropper P, Manning CE (2007) The solubility of corundum in H_2O at high pressure and temperture and its implication for Al mobility in the deep crust and upper mantle. Chem Geol 240:54–60. doi:10.1016/j.chemgeo.2007.01.012

Verdes G, Gout R, Castet S (1992) Thermodynamic properties of the aluminate ion and of bayerite, boemite, diaspore, and gibbsite. Eur J Mineral 4:767–792

Verlaguet A, Brunet F, Goffé B, Murphy WM (2006) Experimental study and modelling of fluid reaction paths in the quartz–kyanite ± muscovite–water system at 0.7 GPa in the 350–550°C range: implications for Al selective transfer during metamorphism. Geochim Cosmochim Acta 70:1772–1788. doi: 10.1016/j.gca.2005.12.014

Walther JV, Helgeson HC (1977) Calculation of the thermodynamic properties of aqueous silica and the solubility of quartz and its polymorphs at high pressure and temperatures. Am J Sci 277:1315–1351

White RW, Powell R, Holland TJB (2007) Progress relating to calculation of partial melting equilibria for metapelites. J Metamorph Geol 25:511–527. doi:10.1111/j.1525-1314.2007.00711.x

Widmer T, Thompson AB (2001) Local origin of high-pressure vein material in eclogite facies rocks of the Zermatt-Saas zone, Switzerland. Am J Sci 301:627–656. doi:10.2475/ajs.301.7.627

Wing BA, Ferry J (2007) Magnitude and geometry of reactive fluid flow from direct inversion of spatial patterns of geochemical alteration. Am J Sci 307:793–832. doi:10.2475/05.2007.02

Wood BJ, Walther JV (1986) Fluid flow during metamorphism and its implications for fluid–rock ratios. In: Walther JV Wood BJ (eds) Fluid–rock interactions during metamorphism, pp 89–108. Springer, New York

Xie Z, Walther JV (1993) Quartz solubilities in NaCl solutions with and without wollastonite at elevated temperatures and pressures. Geochim Cosmochim Acta 57:1947–1955. doi:10.1016/0016-7037(93) 90086-C

Yardley BWD (1977) The nature and significance of the mechanism of sillimanite growth in the Connemara Schists, Ireland. Contrib Mineral Petrol 65:53–58. doi:10.1007/BF00373570

Yardley BWD, Shmulovich KI (1994) An introduction to crustal fluids. In: Shmulovich KI, Yardley BWD, Gonchar GG (eds) Fluids in the crust: equilibrium and transport properties. Chapman & Hall, London, pp 1–12

Zaraisky GP, Soboleva YV (1997) Experimental determination of corundum solubility in aqueous HF solutions at 300 to 600°C and 1 kbar. In: Proceedings of the fifth international symposium on hydrothermal reactions, Gatlinburg, Tennessee, pp 201–205

Zhang YG, Frantz JD (1987) Determination of the homogenisation temperatures and densities of supercritical fluids in the system NaCl–KCl–$CaCl_2$–H_2O using synthetic fluid inclusions. Chem Geol 64:335–350. doi:10.1016/0009-2541(87) 90012-X

Zheng YF (1993) Calculation of oxygen isotope fractionation in anhydrous silicate minerals. Geochim Cosmochim Acta 57:1079–1091. doi:10.1016/0016-7037(93) 90306-H